# Analytical solution of cross- and angle-ply nano plates with strain gradient theory for linear vibrations and buckling



*Published Version:*
Cornacchia, F., Fabbrocino, F., Fantuzzi, N., Luciano, R., Penna, R. (2021). Analytical solution of cross- and angle-ply nano plates with strain gradient theory for linear vibrations and buckling. MECHANICS OF ADVANCED MATERIALS AND STRUCTURES, 28(12), 1201-1215 [10.1080/15376494.2019.1655613].

*Availability:*
This version is available at: https://hdl.handle.net/11585/698729 since: 2024-09-19

*Published:*
DOI: http://doi.org/10.1080/15376494.2019.1655613



(Article begins on next page)

# Analytical solution of cross- and angle-ply nano plates with strain gradient theory for linear vibrations and buckling

F. Cornacchia[1], F. Fabbrocino[2], N. Fantuzzi[1], R. Luciano[3,*], R. Penna[4]

**Abstract**

Vibrations and buckling of Kirchhoff nano plates are investigated using second-order strain gradient theory. The Navier displacement field has been considered for two different sets of boundary conditions and stacking sequences. Different geometries and material properties for isotropic, orthotropic cross- and angle-ply laminates are considered, and numerical simulations are discussed in terms of plate aspect ratio and non local ratio. A comparison with the classical analytical solution is provided whenever possible for buckling loads and fundamental frequencies.

*Keywords:* Stability analysis, Dynamic analysis, Orthotropic laminate, Nano-structures, Nonlocal elastic theory, Analytical modelling

## 1. Introduction

In the current literature MEMS (Micro-Electro-Mechanical-System) and NEMS (Nano-Electro-Mechanical-System) are topics of relevant interest be-

*raimondo.luciano@uniparthenope.it
[1]DICAM Department University of Bologna, Italy
[2]Engineering Department, Pegaso Telematic University, Italy
[3]Engineering Department, Parthenope University, Italy
[4]Department of Civil Engineering, University of Salerno, Italy

cause of their various uses [1, 2, 3]. Indeed, these types of materials can be employed in many areas of application, i.e. engineering, medicine and electronics [4, 2, 5, 6, 7], in the form of generators, transistors, sensors, actuators, resonators, detectors etc.

This work wants to focus the attention on NEMS, which are usually modeled by simulating small scale effects on nano rods, nano beams, nano tubes and nano plates. In fact, the mechanical behavior of nano structural components is size-dependent [8, 9, 10, 11, 12], highly influenced by the material structure and by the interactions at the atomic scale among particles at distant location, as commented in [13, 14, 15, 16, 17, 18, 19, 20, 21], effects that have much lower impact in macro structures. Thus, in order to take into account the size effects, the classical continuum mechanics theories are not suitable, which implies the application of modified versions [22, 23, 24, 25], that are based on the individuation of an internal length scale. A wide range of non classical theories have been developed in order to capture the non locality effects, among which Eringen [26, 26] was one of the pioneer and his nonlocal elasticity theory has been extensively applied in the study of nano structures by scientists [27, 28, 29]. Hence, an important milestone in the practice of higher order theories of linear elasticity is to determine the correct non local relation [30, 31]. A broad list of higher order theories of linear elasticity can be found in literature, among which,strain gradient, modified strain gradient, stress gradient, modified couple stress and micropolar theories can be identified [32**?** , 33, 25, 34, 35, 36, 37, 38, 39], and the choice depends on the research to carry out and on the ability of the scientists. Here, the effort will be focused on the development of studies of buckling and vibrations of nano plates, which is a relevant subject for the scientific community, as it can be found in [40, 41, 42, 43, 44, 45, 46, 47, 48, 49]. An easy theory, which is applied in the present study, is the second order-strain gradient theory that establish a connection between stress and strain of the structure in the constitutive equations through a single non local parameter, as previously done by Papargyri-Beskos [50]. The method followed in the present paper follows the one presented in [51] for static analysis of laminates, where the gap between the theories in terms of deflection and stresses is shown. In fact, the Kirchhoff governing equations in weak form are carried out by considering the size effects, while the Navier displacement field is applied in order to develop the analytical solution in terms of stability and dynamic analysis. Comparison with Reddy [52], Papargyri-Beskos [50] and Babu Patel [21] are provided if possible for the classical continuum mechanics theory, before extending the application to orthotropic laminated materials (cross- and angle-ply laminates) employing the second order-strain gradient theory.

## 2. Theoretical model

### *2.1. Kirchhoff theory*

Different combinations of geometrical and material configurations of orthotropic thin rectangular nanoplates are implemented by making use of the classical laminated plate theory (CLPT). In order to conduct stability and dynamic analysis for such structures, at nano scale level, a modification of the theory, based on the bending plate hypothesis of Kirchhoff is needed. The laminates have dimension $a$ and $b$ along $x$- and $y$-axis, respectively, while the thickness of the generic oriented $k$-th lamina $h_k = z_{k+1} - z_k$, as it is displayed in Fig. 1 For the case of geometric non linearity, the displacements in the three directions can be written from the Kirchhoff assumptions and restrictions as it follows:

$$\begin{aligned} u(x,y,z,t) &= u_0(x,y,t) - z w_{0,x} \\ v(x,y,z,t) &= v_0(x,y,t) - z w_{0,y} \\ w(x,y,z,t) &= w_0(x,y,t) \end{aligned} \tag{1}$$

where, $u_0, v_0, w_0$ are the displacements along $x$-, $y$- and $z$-axis of the points on the mid-surface, and $w_{0,x}$ and $w_{0,y}$ are the homologous rotations.

The plate strain is expressed in the von Karman form:

$$\varepsilon = \left\{\varepsilon^{(m)}\right\} + z\left\{\varepsilon^{(f)}\right\} = \begin{Bmatrix} \varepsilon_{xx}^{(m)} \\ \varepsilon_{yy}^{(m)} \\ \gamma_{xy}^{(m)} \end{Bmatrix} + z \begin{Bmatrix} \varepsilon_{xx}^{(f)} \\ \varepsilon_{yy}^{(f)} \\ \gamma_{xy}^{(f)} \end{Bmatrix} \tag{2}$$

where, $^{(m)}$ indicates the membrane strain, while $^{(f)}$ the flexural strain. $\varepsilon_{xx}$ and $\varepsilon_{yy}$ are the normal strains along $x$ and $y$ directions respectively, instead $\gamma_{xy}$ represents the in-plane shear strain. Consequently, the membrane and flexural strains can be written as function of the displacements:

$$\begin{Bmatrix} \varepsilon_{xx}^{(m)} \\ \varepsilon_{yy}^{(m)} \\ \gamma_{xy}^{(m)} \end{Bmatrix} = \begin{bmatrix} u_{0,x} + \frac{1}{2} w_{0,x}^{2} \\ v_{0,y} + \frac{1}{2} w_{0,y}^{2} \\ u_{0,y} + v_{0,x} + w_{0,x}\, w_{0,y} \end{bmatrix}, \quad \begin{Bmatrix} \varepsilon_{xx}^{(f)} \\ \varepsilon_{yy}^{(f)} \\ \gamma_{xy}^{(f)} \end{Bmatrix} = \begin{bmatrix} -w_{0,xx} \\ -w_{0,yy} \\ -2w_{0,xy} \end{bmatrix} \tag{3}$$

In order to take into account the effects of non locality due to the dimensions of the nano plates, the second-order strain gradient theory must

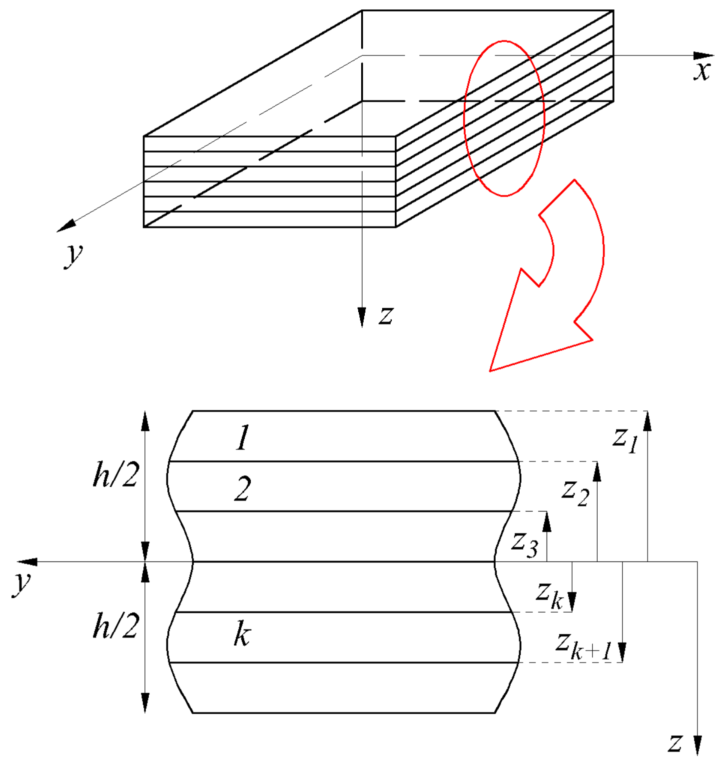


Figure 1: Laminate general layout

be involved in the computation. For the $k$-th orthotropic lamina in terms of laminate coordinates, the constitutive equations can be written as:

$$\begin{Bmatrix} \sigma_{xx} \\ \sigma_{yy} \\ \tau_{xy} \end{Bmatrix}^{(k)} = (1 - \ell^2 \nabla^2) \begin{bmatrix} \bar{Q}_{11} & \bar{Q}_{12} & \bar{Q}_{16} \\ \bar{Q}_{12} & \bar{Q}_{22} & \bar{Q}_{26} \\ \bar{Q}_{16} & \bar{Q}_{26} & \bar{Q}_{66} \end{bmatrix}^{(k)} \begin{Bmatrix} \varepsilon_{xx} \\ \varepsilon_{yy} \\ \gamma_{xy} \end{Bmatrix}^{(k)} \tag{4}$$

where, $\nabla^2 = \partial^2/\partial y^2 + \partial^2/\partial x^2$, and $\bar{Q}_{ij}$ are function of sheets orientations and are derived from the engineering constants in accordance with the formulations below:

$$\begin{aligned} Q_{11} &= \frac{E_1}{1-\nu_{12}\nu_{21}}, \quad Q_{22} = \frac{E_2}{1-\nu_{12}\nu_{21}} \\ Q_{12} &= \frac{E_1\nu_{21}}{1-\nu_{12}\nu_{21}} = \frac{E_2\nu_{12}}{1-\nu_{12}\nu_{21}}, \quad Q_{66} = G_{12} \end{aligned} \tag{5}$$

where, $E_1$, $E_2$ are the Young's moduli, $\nu_{12}$ and $\nu_{21}$ are the Poisson's ratii and $G_{12}$ is the shear modulus.

The dynamic version of the principle of the virtual works (Hamilton's Principle) is employed in order to carry out the equations of motion. It is important to point out that the transverse shear stress, needed for the equilibrium of the plate, has been involved in the boundary conditions and equilibrium of forces.

$$\int_0^T (\delta U + \delta V - \delta K) = 0 \tag{6}$$

with, $\delta U$ is the virtual strain energy, $\delta V$ is the virtual work done by the applied forces, and $\delta K$ is the virtual kinetic energy

Developing the terms in Eq. (6), the Hamilton's Principle can be conveniently written in extended matrix form as:

$$\int_0^T \int_{\Omega_0} \Bigg[ \begin{Bmatrix} \delta u_{0,x} \\ \delta u_{0,y} \\ \delta v_{0,x} \\ \delta v_{0,y} \\ \delta w_{0,xx} \\ \delta w_{0,yy} \\ \delta w_{0,xy} \end{Bmatrix}^T \begin{bmatrix} \mathcal{T}_{11} & \mathcal{T}_{12} & \mathcal{T}_{13} \\ \mathcal{T}_{21} & \mathcal{T}_{22} & \mathcal{T}_{23} \\ \mathcal{T}_{31} & \mathcal{T}_{32} & \mathcal{T}_{33} \\ \mathcal{T}_{41} & \mathcal{T}_{42} & \mathcal{T}_{43} \\ \mathcal{T}_{51} & \mathcal{T}_{52} & \mathcal{T}_{53} \\ \mathcal{T}_{61} & \mathcal{T}_{62} & \mathcal{T}_{63} \\ \mathcal{T}_{71} & \mathcal{T}_{72} & \mathcal{T}_{73} \end{bmatrix} \begin{Bmatrix} u_0 \\ v_0 \\ w_0 \end{Bmatrix}$$

$$- \begin{Bmatrix} \delta w_{0,x} & \delta w_{0,y} \end{Bmatrix} \begin{bmatrix} \hat{N}_{xx} & \hat{N}_{xy} \\ \hat{N}_{xy} & \hat{N}_{yy} \end{bmatrix} \begin{Bmatrix} w_{0,x} \\ w_{0,y} \end{Bmatrix} \tag{7}$$

$$+ \begin{Bmatrix} \delta \ddot{u}_0 \\ \delta \ddot{v}_0 \\ \delta \ddot{w}_0 \\ \delta \ddot{w}_{0,x} \\ \delta \ddot{w}_{0,y} \end{Bmatrix}^T \begin{bmatrix} I_0 & 0 & 0 & -I_1 & 0 \\ 0 & I_0 & 0 & 0 & -I_1 \\ 0 & 0 & I_0 & 0 & 0 \\ -I_1 & 0 & 0 & I_2 & 0 \\ 0 & -I_1 & 0 & 0 & I_2 \end{bmatrix} \begin{Bmatrix} u_0 \\ v_0 \\ w_0 \\ w_{0,x} \\ w_{0,y} \end{Bmatrix} \Bigg] dxdy \Bigg] dt$$

$$+ \text{ boundary integral terms} = 0$$

where the variational form of the displacement field is dentified by $\delta$, while its corresponding derivatives in time by the dots, the terms $\mathcal{T}$ are shown in the appendix, $\hat{N}_{xx}, \hat{N}_{yy}, \hat{N}_{xy}$ identify the axial and shear buckling terms and $I_0, I_1, I_2$ are the mass inertias which can be defined as it follows:

$$I_i = \rho \sum_{k=1}^{N} \int_{z_k}^{z_{k+1}} z^i \, dz \tag{8}$$

where, $i = 0, 1, 2$. The following resultants of forces and moments are obtained by integrating the stresses for each layer through the $z$-axis:

$$\begin{Bmatrix} N_{xx} \\ N_{yy} \\ N_{xy} \end{Bmatrix} = (1-\ell^2\nabla^2)\left( \begin{bmatrix} A_{11} & A_{12} & A_{16} \\ A_{12} & A_{22} & A_{26} \\ A_{16} & A_{26} & A_{66} \end{bmatrix} \begin{Bmatrix} \varepsilon_{xx}^{(m)} \\ \varepsilon_{yy}^{(m)} \\ \gamma_{xy}^{(m)} \end{Bmatrix} + \begin{bmatrix} B_{11} & B_{12} & B_{16} \\ B_{12} & B_{22} & B_{26} \\ B_{16} & B_{26} & B_{66} \end{bmatrix} \begin{Bmatrix} \varepsilon_{xx}^{(f)} \\ \varepsilon_{yy}^{(f)} \\ \gamma_{xy}^{(f)} \end{Bmatrix} \right) \tag{9}$$

$$\begin{Bmatrix} M_{xx} \\ M_{yy} \\ M_{xy} \end{Bmatrix} = (1-\ell^2\nabla^2)\left( \begin{bmatrix} B_{11} & B_{12} & B_{16} \\ B_{12} & B_{22} & B_{26} \\ B_{16} & B_{26} & B_{66} \end{bmatrix} \begin{Bmatrix} \varepsilon_{xx}^{(m)} \\ \varepsilon_{yy}^{(m)} \\ \gamma_{xy}^{(m)} \end{Bmatrix} + \begin{bmatrix} D_{11} & D_{12} & D_{16} \\ D_{12} & D_{22} & D_{26} \\ D_{16} & D_{26} & D_{66} \end{bmatrix} \begin{Bmatrix} \varepsilon_{xx}^{(f)} \\ \varepsilon_{yy}^{(f)} \\ \gamma_{xy}^{(f)} \end{Bmatrix} \right) \tag{10}$$

where, the stiffnesses are computed as it follows:

$$\begin{aligned} A_{ij} &= \sum_{k=1}^{N} \bar{Q}_{ij}^{(k)}(z_{k+1} - z_k) \\ B_{ij} &= \frac{1}{2}\sum_{k=1}^{N} \bar{Q}_{ij}^{(k)}(z_{k+1}^2 - z_k^2) \\ D_{ij} &= \frac{1}{3}\sum_{k=1}^{N} \bar{Q}_{ij}^{(k)}(z_{k+1}^3 - z_k^3) \end{aligned} \tag{11}$$

The linear equations of motion of the classical laminated plate theory in terms of displacement, accounting for non local effects are obtained by setting the non linear terms equal to zero and by carrying out integration by parts in (7):

$$
\begin{gathered}
A_{11}u_{0},_{xx} + 2A_{16}u_{0},_{xy} + A_{66}u_{0},_{yy} + A_{16}v_{0},_{xx} + (A_{12} + A_{66})v_{0},_{xy} + A_{26} \\
v_{0},_{yy} - \big[B_{11}w_{0},_{xxx} + 3B_{16}w_{0},_{xxy} + (B_{12} + 2B_{66})w_{0},_{xyy} + B_{26}w_{0},_{yyy}\big] - \ell^2\big[A_{11} \\
\big(u_{0},_{xxxx} + u_{0},_{xxyy}\big) + 2A_{16}\big(u_{0},_{xxxy} + u_{0},_{xyyy}\big) + A_{66}\big(u_{0},_{xxyy} + u_{0},_{yyyy}\big) + A_{16} \\
\big(v_{0},_{xxxx} + v_{0},_{xxyy}\big) + (A_{12} + A_{66})\big(v_{0},_{xxxy} + v_{0},_{xyyy}\big) + A_{26}\big(v_{0},_{xxyy} + v_{0},_{yyyy}\big) - \\
- \big[B_{11}\big(w_{0},_{xxxxx} + w_{0},_{xxxyy}\big) + 3B_{16}\big(w_{0},_{xxxxy} + w_{0},_{xxyyy}\big) + (B_{12} + 2B_{66}) \\
\big(w_{0},_{xxxyy} + w_{0},_{xyyyy}\big) + B_{26}\big(w_{0},_{xxyyy} + w_{0},_{yyyyy}\big)\big]\big] = I_0\ddot{u}_0 - I_1\ddot{w}_{0},_{x}
\end{gathered}
\tag{12}
$$

$$
\begin{gathered}
A_{16}u_{0},_{xx} + (A_{12} + A_{66})u_{0},_{xy} + A_{26}u_{0},_{yy} + A_{66}v_{0},_{xx} + 2A_{26}v_{0},_{xy} + A_{22} \\
v_{0},_{yy} - \big[B_{16}w_{0},_{xxx} + (B_{12} + 2B_{66})w_{0},_{xxy} + 3B_{26}w_{0},_{xyy} + B_{22}w_{0},_{yyy}\big] - \ell^2\big[A_{16} \\
\big(u_{0},_{xxxx} + u_{0},_{xxyy}\big) + (A_{12} + A_{66})\big(u_{0},_{xxxy} + u_{0},_{xyyy}\big) + A_{26}\big(u_{0},_{xxyy} + u_{0},_{yyyy}\big) + \\
+ A_{66}\big(v_{0},_{xxxx} + v_{0},_{xxyy}\big) + 2A_{26}\big(v_{0},_{xxxy} + v_{0},_{xyyy}\big) + A_{22}\big(v_{0},_{xxyy} + v_{0},_{yyyy}\big) - \\
- \big[B_{16}\big(w_{0},_{xxxxx} + w_{0},_{xxxyy}\big) + (B_{12} + 2B_{66})\big(w_{0},_{xxxxy} + w_{0},_{xxyyy}\big) + 3B_{26} \\
\big(w_{0},_{xxxyy} + w_{0},_{xyyyy}\big) + B_{22}\big(w_{0},_{xxyyy} + w_{0},_{yyyyy}\big)\big]\big] = I_0\ddot{v}_0 - I_1\ddot{w}_{0},_{y}
\end{gathered}
\tag{13}
$$

$$
\begin{aligned}
&B_{11}u_{0,xxx} + 3B_{16}u_{0,xxy} + (B_{12}+2B_{66})u_{0,xyy} + B_{26}u_{0,yyy} + B_{16}v_{0,xxx} + (B_{12}+\\
&+2B_{66})v_{0,xxy} + 3B_{26}v_{0,xyy} - B_{22}v_{0,yyy} - \big[D_{11}w_{0,xxxx} + 4D_{16}w_{0,xxxy} + 2(D_{12}+\\
&+2D_{66})w_{0,xxyy} + 4D_{26}w_{0,xyyy} + D_{22}w_{0,yyyy}\big] - \ell^2\big[B_{11}\big(u_{0,xxxxx} + u_{0,xxxyy}\big)+\\
&+3B_{16}\big(u_{0,xxxxy} + u_{0,xxyyy}\big) + (B_{12}+2B_{66})\big(u_{0,xxxyy} + u_{0,yyyy}\big) + B_{26}\\
&\big(u_{0,xxyyy} + u_{0,yyyyy}\big) + B_{16}\big(v_{0,xxxxx} + v_{0,xxxyy}\big) + (B_{12}+2B_{66})\big(v_{0,xxxxy}+\\
&+v_{0,xxyyy}\big) + 3B_{26}\big(v_{0,xxxyy} + v_{0,xyyyy}\big) + B_{22}\big(v_{0,xxyyy} + v_{0,yyyyy}\big) - \big[D_{11}\\
&\big(w_{0,xxxxxx} + w_{0,xxxxyy}\big) + 4D_{16}\big(w_{0,xxxxxy} + w_{0,xxxyyy}\big) + 2(D_{12}+2D_{66})\\
&\big(w_{0,xxxxyy} + w_{0,xxyyyy}\big) + 4D_{26}\big(w_{0,xxxyyy} + w_{0,xyyyyy}\big) + D_{22}\big(w_{0,xxyyyy}+\\
&+w_{0,yyyyyy}\big)\big]\big] = I_1\big(\ddot{u}_{0,x} + \ddot{v}_{0,y}\big) + I_0\ddot{w}_0 - I_2\big(\ddot{w}_{0,xx} + \ddot{w}_{0,yy}\big) - \big(\hat{N}_{xx}w_{0,xx}+\\
&+2\hat{N}_{xy}w_{0,xy} + \hat{N}_{yy}w_{0,yy}\big)
\end{aligned}
\tag{14}
$$

### *2.2. Navier solution*

In this section, the Navier procedure for simply supported laminates is applied to orthotropic cross ply and angle ply laminates. By replacing the Navier displacement field, which will be made explicit in the corresponding subsections, in the system below (omitting the von Karman non linear terms) the analytical solutions are obtained:

$$
\begin{bmatrix} \hat{c}_{11} & \hat{c}_{12} & \hat{c}_{13} \\ \hat{c}_{12} & \hat{c}_{22} & \hat{c}_{23} \\ \hat{c}_{13} & \hat{c}_{23} & \hat{c}_{33}+\hat{s}_{33} \end{bmatrix}
\begin{Bmatrix} U_{mn} \\ V_{mn} \\ W_{mn} \end{Bmatrix}
+
\begin{bmatrix} \hat{m}_{11} & 0 & \hat{m}_{13} \\ 0 & \hat{m}_{22} & \hat{m}_{23} \\ \hat{m}_{13} & \hat{m}_{23} & \hat{m}_{33} \end{bmatrix}
\begin{Bmatrix} \ddot{U}_{mn} \\ \ddot{V}_{mn} \\ \ddot{W}_{mn} \end{Bmatrix}
=
\begin{Bmatrix} 0 \\ 0 \\ 0 \end{Bmatrix}
\tag{15}
$$

where, the terms in the matrices will be made explicit for cross- and angle-ply laminates.

The analytical solutions for the stability and dynamic analysis respectively, are carried out and shown below:

$$\bar{N} = \frac{1}{\alpha^2 + k\beta^2}\left(\hat{c}_{33} + \hat{c}_{13}\frac{a_1}{a_0} + \hat{c}_{23}\frac{a_2}{a_0}\right) \tag{16}$$

$$\bar{\omega}^2 = \frac{1}{\hat{m}_{33}}\left(\hat{c}_{33} + \hat{c}_{13}\frac{a_1}{a_0} + \hat{c}_{23}\frac{a_2}{a_0}\right) \tag{17}$$

where

$$\begin{aligned} a_{mn} &= \hat{c}_{33} + \hat{c}_{13}\frac{a_1}{a_0} + \hat{c}_{23}\frac{a_2}{a_0} \\ a_0 &= \hat{c}_{11}\hat{c}_{22} - \hat{c}_{12}\hat{c}_{12} \\ a_1 &= \hat{c}_{12}\hat{c}_{23} - \hat{c}_{13}\hat{c}_{22} \\ a_2 &= \hat{c}_{13}\hat{c}_{12} - \hat{c}_{11}\hat{c}_{23} \end{aligned} \tag{18}$$

*2.2.1. Antisymmetric Cross-Ply Laminates*

The Navier displacement field is assumed to be:

$$\begin{aligned} u_0(x,y) &= \sum_{n=1}^{\infty}\sum_{m=1}^{\infty} U_{mn}\cos\alpha x\sin\beta y \\ v_0(x,y) &= \sum_{n=1}^{\infty}\sum_{m=1}^{\infty} V_{mn}\sin\alpha x\cos\beta y \\ w_0(x,y) &= \sum_{n=1}^{\infty}\sum_{m=1}^{\infty} W_{mn}\sin\alpha x\sin\beta y \end{aligned} \tag{19}$$

where, $\alpha = m\pi/a$ and $\beta = n\pi/b$

in order to satisfy the displacement boundary conditions (SS-1), as it follows:

$$
\begin{aligned}
u_0(x,0,t)=0, u_0(x,b,t)=0, v_0(0,y,t)=0, v_0(a,y,t)=0 \\
w_0(x,0,t)=0, w_0(x,b,t)=0, w_0(0,y,t)=0, w_0(a,y,t)=0 \\
\left.\frac{\partial w_0}{\partial x}\right|_{(x,0,t)}=0, \left.\frac{\partial w_0}{\partial x}\right|_{(x,b,t)}=0, \left.\frac{\partial w_0}{\partial y}\right|_{(0,y,t)}=0, \left.\frac{\partial w_0}{\partial y}\right|_{(a,y,t)}=0,
\end{aligned} \tag{20}
$$

The coefficients to be used in Eq. (15), for the cross-ply laminate case are shown below:

$$
\begin{aligned}
\hat{c}_{11} =& -(\alpha^2 A_{11}+\beta^2 A_{66})-\ell^2[\alpha^4 A_{11}+\alpha^2\beta^2(A_{11}+A_{66})+\beta^4 A_{66}] \\
\hat{c}_{12} =& -\alpha\beta(A_{12}+A_{66})-\ell^2[\alpha^3\beta(A_{12}+A_{66})+\alpha\beta^3(A_{12}+A_{66})] \\
\hat{c}_{13} =& [\alpha^3 B_{11}+\alpha\beta^2(B_{12}+2B_{66})]+\ell^2[\alpha^5 B_{11}+\alpha^3\beta^2(B_{11}+B_{12}+2B_{66})+ \\
& +\alpha\beta^4(B_{12}+2B_{66})] \\
\hat{c}_{22} =& -(\alpha^2 A_{66}+\beta^2 A_{22})-\ell^2[\alpha^4 A_{66}+\alpha^2\beta^2(A_{22}+A_{66})+\beta^4 A_{22}] \\
\hat{c}_{23} =& [\beta^3 B_{22}+\alpha^2\beta(B_{12}+2B_{66})]+\ell^2[\beta^5 B_{22}+\alpha^2\beta^3(B_{22}+B_{12}+2B_{66})+ \\
& +\alpha^4\beta(B_{12}+2B_{66})] \\
\hat{c}_{33} =& -(\alpha^4 D_{11}+\beta^4 D_{22}+2\alpha^2\beta^2(D_{12}+2D_{66}))-\ell^2[\alpha^6 D_{11}+\beta^6 D_{22}+\alpha^4\beta^2 \\
& (D_{11}+2D_{12}+4D_{66})+\alpha^2\beta^4(D_{22}+2D_{12}+4D_{66})]
\end{aligned} \tag{21}
$$

$$
\begin{aligned}
\hat{m}_{11} &= \hat{m}_{22} = I_0 \\
\hat{m}_{13} &= -I_1\alpha \\
\hat{m}_{23} &= -I_1\beta \\
\hat{m}_{33} &= I_0 + I_2(\alpha^2+\beta^2) \\
\hat{s}_{33} &= (\alpha^2\hat{N}_{xx}+\beta^2\hat{N}_{yy})
\end{aligned} \tag{22}
$$

It is important to point out that, the solution for cross ply laminated with SS-1 boundary conditions is valid only if:

$$A_{16} = A_{26} = B_{16} = B_{26} = D_{16} = D_{26} = 0 \tag{23}$$

*2.2.2. Antisymmetric Angle-Ply Laminates*

The Navier displacement field for this case, is assumed to be:

$$\begin{aligned} u_0(x,y) &= \sum_{n=1}^{\infty}\sum_{m=1}^{\infty} U_{mn} \sin\alpha x \cos\beta y \\ v_0(x,y) &= \sum_{n=1}^{\infty}\sum_{m=1}^{\infty} V_{mn} \cos\alpha x \sin\beta y \\ w_0(x,y) &= \sum_{n=1}^{\infty}\sum_{m=1}^{\infty} W_{mn} \sin\alpha x \sin\beta y \end{aligned} \tag{24}$$

which satisfies the SS-2 boundary conditions:

$$\begin{aligned} u_0(0,y,t) = 0, u_0(a,y,t) = 0, v_0(x,0,t) = 0, v_0(x,b,t) = 0 \\ w_0(x,0,t) = 0, w_0(x,b,t) = 0, w_0(0,y,t) = 0, w_0(a,y,t) = 0 \\ \left.\frac{\partial w_0}{\partial x}\right|_{(x,0,t)} = 0, \left.\frac{\partial w_0}{\partial x}\right|_{(x,b,t)} = 0, \left.\frac{\partial w_0}{\partial y}\right|_{(0,y,t)} = 0, \left.\frac{\partial w_0}{\partial y}\right|_{(a,y,t)} = 0, \end{aligned} \tag{25}$$

where $\alpha$ and $\beta$ are already defined in the previous subsection.

In this case, the coefficient to be employed in Eq. (15), are the following:

$$
\begin{aligned}
\hat{c}_{11} &= A_{11}\alpha^2 + A_{66}\beta^2 + \ell^2[A_{11}(\alpha^4 + \alpha^2\beta^2) + A_{66}(\beta^4 + \alpha^2\beta^2)] \\
\hat{c}_{12} &= (A_{12} + A_{66})\alpha\beta + \ell^2(A_{12} + A_{66})(\alpha\beta^3 + \alpha^3\beta) \\
\hat{c}_{13} &= -(3B_{16}\alpha^2\beta + B_{26}\beta^3) - \ell^2[3B_{16}(\alpha^4\beta + \alpha^2\beta^3) + B_{26}(\alpha^2\beta^3 + \beta^5)] \\
\hat{c}_{22} &= A_{66}\alpha^2 + A_{22}\beta^2 + \ell^2[A_{66}(\alpha^4 + \alpha^2\beta^2) + A_{22}(\beta^4 + \alpha^2\beta^2)] \\
\hat{c}_{23} &= -(B_{16}\alpha^3 + 3B_{26}\alpha\beta^2) - \ell^2[B_{16}(\alpha^5 + \alpha^3\beta^2) + 3B_{26}(\alpha\beta^4 + \alpha^3\beta^2)] \\
\hat{c}_{33} &= D_{11}\alpha^4 + 2(D_{12} + 2D_{66})\alpha^2\beta^2 + D_{22}\beta^4 + \ell^2[D_{11}(\alpha^6 + \alpha^4\beta^2) + 2(D_{12} + \\
&\quad + 2D_{66})(\alpha^4\beta^2 + \alpha^2\beta^4) + D_{22}(\alpha^2\beta^4 + \beta^6)]
\end{aligned} \tag{26}
$$

$$
\begin{aligned}
\hat{m}_{11} &= \hat{m}_{22} = I_0 \\
\hat{m}_{33} &= I_0 + I_2(\alpha^2 + \beta^2) \\
\hat{m}_{23} &= \hat{m}_{13} = 0 \\
\hat{s}_{33} &= (\alpha^2\hat{N}_{xx} + \beta^2\hat{N}_{yy})
\end{aligned} \tag{27}
$$

Finally, the SS-2 boundary conditions exsist only if the stiffness:

$$
A_{16} = A_{26} = B_{11} = B_{12} = B_{22} = B_{66} = D_{16} = D_{26} = 0 \tag{28}
$$

## 3. Results - Stability analysis

### *3.1. Isotropic*

Firstly, the outcomes for an isotropic single lamina were carried out in order to make the comparison with Papargyri et al. [50] for the case of buckling, assuming gradient elastic material behavior. The lamina is assumed to be simply supported, with the same dimensions along the $x$ and $y$ directions

($a = b$), while the properties of the isotropic material are: $E_1 = E_2 = E = 1$ ($E_2$ is always considered equal to one in the computations and $E_1$ will vary for cross- and angle-plies), $\nu = 0.25$ and $G = 0.5E/(1+\nu)$. The solution in terms of buckling load, for uniaxial compression in $x$ direction, which accounts for non locality effects, is dimensionless with respect to the classical solution ($\ell = 0$). Thus, in the graph below the dimensionless buckling load $\bar{N}$ is plotted as a function of the normalized gradient coefficient $(\ell/a)^2$, where the dots represent the solution of the Eq. (16), while the solid line is the computation of the reference equation from Ref. [50], obtained for $n = m = 1$ which correspond to the minimum value for square plates:

$$\bar{N} = \left[1 + 2\pi^2\left(\frac{\ell}{a}\right)^2\right] \tag{29}$$

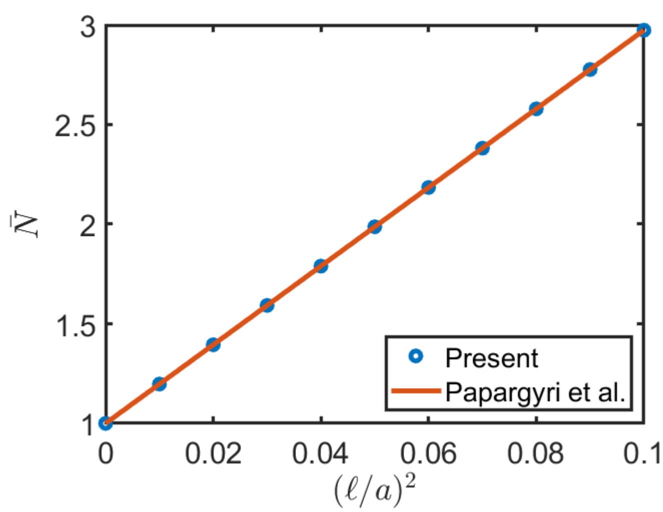


Figure 2: Buckling - comparison with Ref. [50].

The Figure 2 shows how in good agreement are the formulations. The rising trend displays that the critical buckling load grows with non local ratio $(\ell/a)^2$. Note that the minimum buckling load does not always occur for $m = n = 1$ for rectangular and laminated plate configurations as it will be discussed in the following. For this reason the minimum buckling load has been observed to occur within $m, n = 1, 2, 3$ in the present computations.

Once Eq. (16) has been verified, it is employed in order to understand the behavior to changing aspect ratios $a/b$. The material properties are the same as the previous case, beside the classical theory $(\ell/a)^2 = 0.00$, two more values of non local ratios are analized $(\ell/a)^2 = 0.05$ and $(\ell/a)^2 = 0.10$, while the compression is considered for uniaxial and biaxial cases, $k = 0$ and $k = 1$, respectively. It is important to point out that, using the Navier displacement field only the uniaxial and biaxial cases can be studied, while not the tangential buckling because the equations cannot work in this case.

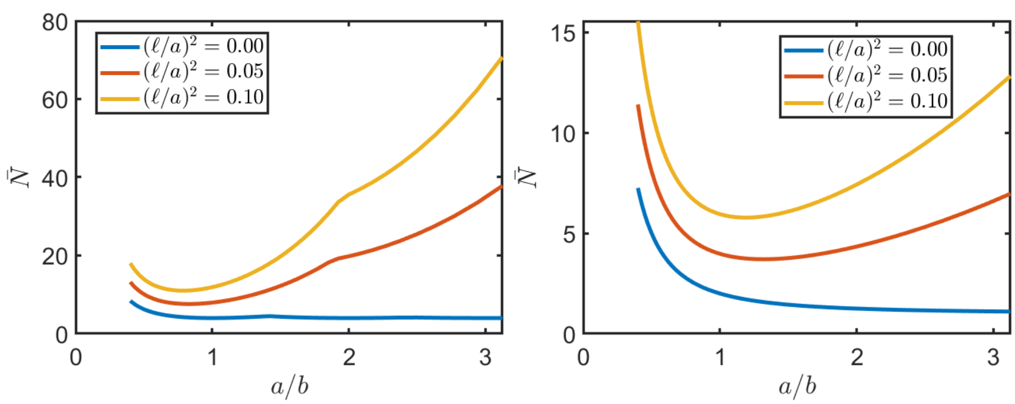


a) b)

Figure 3: Nondimensionalized buckling load versus plate aspect ratio for isotropic lamina - a)Uniaxial compression, b)Biaxial compression

From the graph of uniaxial compression, it is possible to see how for the classical theory, after an initial decrising of dimensionless buckling load with $a/b$, the solution has stabilized behavior and quite smooth trend. On the other hand, if non local effects are involved in the computation, rising paths are shown since values lower than $a/b = 1$ after the initial decreasing. Moreover, discontinuities in both trends are displayed for $a/b$ slight lower than two. From the second graph of Fig. 3, smooth paths are shown for the three cases and all of them have declining trend in the first phase. Then, the classical theory presents almost constant $\bar{N}$ since $a/b$ around unity, while when the lamina is treated with second order theory, it answers with rising $\bar{N}$ to changing $a/b$.

In both cases, for the whole range of lamina dimensions taken into account, higher are the values of $(\ell/a)^2$ higher are the critical load magnitudes, moreover increasing gap between classical and non local theory to rising $a/b$ are displayed.

### *3.2. Antisymmetric cross-ply*

Secondly, othotropic cross-ply plates are studied. For the classical theory the comparison with Reddy [52] is provided whenever possible, then the application is extended to the second order theory, presenting outcomes for $(\ell/a)^2$ equal to 0.05 and 0.10. The ratio $E_1/E_2$ assumes different magnitudes, which will be given step by step, while $\nu_{12} = 0.25$, $G_{12} = G_{13} = 0.5E_2$ and $G_{23} = 0.2E_2$ are the same during the computation. In the first two sections of the tables 1 and 2, Reddy and present outcomes are reported for the classical theory, then the application is applied to $(\ell/a)^2$ equal to 0.05 and 0.10. The aspect ratios $a/b$ treated are: 0.5, 1.0 and 1.5, while $E_1/E_2$ ratio assumes magnitudes equal to 5, 10, 20, 25 and 40, for $0/90/0/90 = (0/90)_2$ laminate layout. Buckling loads have been reported in dimensionless form as

| | | $E_1/E_2$ | | | | |
|---|---|---|---|---|---|---|
| | $a/b$ | 5 | 10 | 20 | 25 | 40 |
| Reddy [52] | 0.5 | 4.705 | 4.157 | 3.828 | 3.757 | 3.647 |
| | 1 | 2.643 | 2.189 | 1.923 | 1.866 | 1.778 |
| | 1.5 | 2.955 | 2.487 | 2.211 | 2.152 | 2.061 |
| $(\ell/a)^2 = 0.00$ | 0.5 | 4.705 | 4.157 | 3.828 | 3.757 | 3.647 |
| | 1 | 2.643 | 2.189 | 1.923 | 1.866 | 1.778 |
| | 1.5 | 2.955 | 2.487 | 2.211 | 2.152 | 2.061 |
| $(\ell/a)^2 = 0.05$ | 0.5 | 7.667 | 6.778 | 6.234 | 6.115 | 5.927 |
| | 1 | 5.422 | 4.546 | 3.994 | 3.868 | 3.661 |
| | 1.5 | 8.952 | 7.769 | 6.968 | 6.772 | 6.441 |
| $(\ell/a)^2 = 0.10$ | 0.5 | 10.600 | 9.374 | 8.623 | 4.232 | 8.199 |
| | 1 | 8.131 | 6.830 | 6.0138 | 2.281 | 5.516 |
| | 1.5 | 14.500 | 12.617 | 11.340 | 3.340 | 10.486 |

Table 1: Uniaxial buckling loads ($k = 0$) for $(0/90)_2$ laminate configuration

it follows: $\bar{N} = N_{cr}[b^2/(\pi^2 D_{22})]$, considering as maximum order of expansion $m, n = 1, 2, 3$ because the critical buckling load was sought. Table 1 is referred to uniform uniaxial compression ($k = 0$), instead table 2 to biaxial one ($k = 1$).

In both Tab. 1 and 2 it is possible to see how results match accurately in the classic application, whereas as it was expected an increasing of the magnitude of the buckling loads is shown for the second order gradient theory. Moreover, it is complicated to make a comparison in terms of variable $E_1/E_2$ and $a/b$ parameter, due to the fluctuating trends within the same theory,

| | | $E_1/E_2$ | | | | |
|---|---|---|---|---|---|---|
| | $a/b$ | 5 | 10 | 20 | 25 | 40 |
| Reddy [52] | 0.5 | 3.764 | 3.325 | 3.062 | 3.005 | 2.917 |
| | 1 | 1.322 | 1.095 | 0.962 | 0.933 | 0.889 |
| | 1.5 | 1.009 | 0.860 | 0.773 | 0.754 | 0.725 |
| $(\ell/a)^2 = 0.00$ | 0.5 | 3.764 | 3.325 | 3.062 | 3.005 | 2.917 |
| | 1 | 1.322 | 1.095 | 0.962 | 0.933 | 0.889 |
| | 1.5 | 1.009 | 0.860 | 0.773 | 0.754 | 0.725 |
| $(\ell/a)^2 = 0.05$ | 0.5 | 6.134 | 5.423 | 4.987 | 4.892 | 4.742 |
| | 1 | 2.711 | 2.273 | 1.997 | 1.934 | 1.830 |
| | 1.5 | 2.754 | 2.390 | 2.144 | 2.084 | 1.982 |
| $(\ell/a)^2 = 0.10$ | 0.5 | 8.480 | 7.499 | 6.899 | 6.767 | 6.559 |
| | 1 | 4.065 | 3.415 | 3.007 | 2.913 | 2.758 |
| | 1.5 | 4.462 | 3.882 | 3.489 | 3.393 | 3.226 |

Table 2: Biaxial buckling loads ($k = 1$) for $(0/90)_2$ laminate configuration

especially for $k = 0$. Thus, in order to draw conclusions it is needed to represent outcomes in graphical form, wherein material properties chosen for the analysis are: $E_1/E_2 = 25$ and $E_1/E_2 = 40$. The laminate configurations studied are: $(0/90)$, $(0/90)_2$ and $(0/90)_4$ for the uniform uniaxial compression $(k = 0)$, while for the biaxial case $(0/90)$, $(0/90)_2$ and $(0/90)_3$ are taken into account. The dimensionless expression used, is again: $\bar{N} = N_{cr}[b^2/(\pi^2 D_{22})]$, with a maximum expansion order of $m, n = 1, 2, 3$.

In Fig. 4 and 5, it is possible to see how the classical theory displays the lower critical loads for every laminate configuration, material and uniform compression type. It shows also discontinuities for the uniaxial compression, instead smooth trends for biaxial one, because the buckling load is not given by $m = n = 1$ for rectangular plates as discussed in classical references [52]. Moreover, for both classical and second gradient order theories, an initial reduction of the buckling load is shown, in the first case it is followed by a quite constant path, while for the second case it is visible the growing magnitude with increasing value of aspect ratio, where slope expands with non local ratios. Laminae made by the same sequence of layers, but accounting for different materials are studied and it comes out that if $E_1/E_2 = 25$ is considered as property of the material, an higher magnitude of buckling load is displaced compared to $E_1/E_2 = 40$ case. From the comparison among different layouts for both uniaxial and biaxial compression, it comes out that, to parity of materials and plate thickness, the lower critical load belongs to $(0/90)$ configuration, while its value grows as more layers are added to the plate.

| | $E_1/E_2$ | 10 | 25 | 40 |
|---|---|---|---|---|
| $(45/-45)$ | Reddy [52] | 9.066 | 15.476 | 21.709 |
| | $(\ell/a)^2 = 0.00$ | 9.066 | 15.476 | 21.709 |
| | $(\ell/a)^2 = 0.05$ | 18.015 | 30.750 | 43.135 |
| | $(\ell/a)^2 = 0.10$ | 26.963 | 46.024 | 64.561 |
| $(45/-45)_4$ | Reddy [52] | 17.637 | 41.163 | 64.683 |
| | $(\ell/a)^2 = 0.00$ | 17.637 | 41.163 | 64.683 |
| | $(\ell/a)^2 = 0.05$ | 35.043 | 81.789 | 128.522 |
| | $(\ell/a)^2 = 0.10$ | 52.450 | 122.415 | 192.362 |

Table 3: Uniaxial buckling loads for $(45/-45)$ and $(45/-45)_4$ laminate configurations

### *3.3. Antisymmetric angle-ply*

Finally, in this section orthotropic angle-ply laminates are studied. As in the previous case in tables 3 and 4, the first two sections are referred to the comparison with Reddy of the classical theory [52], then it is extended to the second-order strain gradient theory. All the parameters employed can be picked from the previous paragraph, except the laminates taken into account which are: $(45/-45)$ and $(45/-45)_4$, while the $E_1/E_2$ ratios are specified in the tables. Both uniform uniaxial ($k = 0$) and biaxial ($k = 1$) compression of the square plate, along $x$, and $x$ and $y$ are carried out, using the following dimensionless expression: $\bar{N} = N_{cr}[b^2/(h^3E_2)]$.

From both Tab 3 and 4, the comparison for the classical theory leads to good confidence in the method also for orthotropic antisymmetric angle-ply laminates. Moreover, as in the earlier case it is possible to see an increasing in magnitude of the dimensionless buckling load to rising $(\ell/a)^2$. Consequently,

| | $E_1/E_2$ | 10 | 25 | 40 |
|---|---|---|---|---|
| $(45/-45)$ | Reddy [52] | 4.533 | 7.738 | 10.854 |
| | $(\ell/a)^2 = 0.00$ | 4.533 | 7.738 | 10.854 |
| | $(\ell/a)^2 = 0.05$ | 9.007 | 15.375 | 21.567 |
| | $(\ell/a)^2 = 0.10$ | 13.481 | 23.012 | 32.280 |
| $(45/-45)_4$ | Reddy [52] | 8.818 | 20.581 | 32.341 |
| | $(\ell/a)^2 = 0.00$ | 8.818 | 20.581 | 32.341 |
| | $(\ell/a)^2 = 0.05$ | 17.522 | 40.895 | 64.261 |
| | $(\ell/a)^2 = 0.10$ | 26.225 | 61.208 | 96.181 |

Table 4: Biaxial buckling loads for $(45/-45)$ and $(45/-45)_4$ laminate configurations

as it follows, a deeper study in order to catch the trend of $(-45/45)_i$, (with $i = 1, 2, 3, 4$) laminate configurations is carried out, enlarging the range of $a/b$ up to five and considering $E_1/E_2$ equal to 25 and 40, in both $k = 0$ and $k = 1$ conditions.

As for the cross-ply laminates, the figures 6 and 7 show higher values of dimensionless buckling load for values of non local ratio equal to 0.10. Also, when $k = 0$ the classical theory displays flat trends, differently from the second-order strain gradient theory which presents rough tendency, instead if $k = 1$ they are always smooth. The behavior in case of $(\ell/a)^2 = 0$ presents an original decreasing followed by a stable trend, viceversa if $(\ell/a)^2$ is non zero the consecutive part grows up to very high values. In addition, comparing the different behavior of the plates it is possible to assert that to parity of material, the six-layered plate shows much higher critical load for every $a/b$, and comparing the two-, four- and six-layered laminate in $k = 0$ and $k = 1$

it is possible to see that for uniaxial case the structures buckles for much higher values.

# 4. Results - Dynamic analysis

## *4.1. Isotropic*

Accordingly to what previously done for the stability analysis, also for the free vibration analysis the first step is to compare the present solution to the Papargyri et al. [50], which is expressed by Eq.(30) for isotropic materials. The material properties, of the square plate ($a = b$), are the following: $E_1/E_2 = 1$, $\nu = 0.25$ and $G = 0.5E/(1+\nu)$. The dimensionless frequency $\bar{\omega}$

$$\bar{\omega} = \sqrt{1 + 2\pi^2\left(\frac{\ell}{a}\right)^2} \tag{30}$$

has been plotted for changing dimensionless $(\ell/a)^2$, for $n = m = 1$. In Fig. 8 it is possible to see how outcomes match accurately, where the dots represent the solution of the Eq. (17), and the solid line is referred to the computation of Eq. (30), showing a rising parabolic behavior for the range of $(\ell/a)^2$ within 0 and 0.1. Thus, the study has been extended in order to understand the behavior for different plate geometries. In fact, outcomes are plotted in Fig. 9 considering an isotropic lamina, for non local ratios equal to 0, 0.05 and 0.10.

It is possible to see an increasing of the dimensionless frequency magnitude with $(\ell/a)^2$, for the whole path, showing higher gaps among theories as $a/b$ rises. Moreover, the initial decreasing is followed by a stable trend for the classical theory ($(\ell/a)^2 = 0$) and by a rising one for the second-order strain gradient theory.

### 4.2. Antisymmetric cross-ply

Then, analysis continues facing to antisymmetric cross-ply laminates. Whenever it has been possible, comparisons with Reddy [52] are carried out for $(\ell/a)^2 = 0$, then results are extended to second-order strain gradient theory. In table 5, dimensionless frequencies of square antisymmetric cross-ply laminates (layouts: (0/90), $(0/90)_2$ and $(0/90)_4$) are carried out imposing $m, n = 1, 2, 3$. The comparison with Reddy [52] is provided in its first two sections for the classical theory, then the theory has been developed also for $(\ell/a)^2$ equal to 0.05 and 0.10. The material properties are given: $E_1/E_2$ equal to 10 and 20, $\nu_{12} = 0.25$, $G_{12} = G_{13} = 0.5E_2$ and $G_{23} = 0.2E_2$. The frequency is dimensionless with respect to the following formula: $\bar{\omega} = \omega b^2/\pi^2\sqrt{\rho h/D_{22}}$.

In Tab. 5 is it possible to see how results are in good agreement for what concerns the classical theory. Moreover, $\bar{\omega}$ increases with the number of layers in the laminate accounting for the same total thickness, for every mode and value of non local ratio. Thus, graphic results are drawn, for (0/90), $(0/90)_2$ and $(0/90)_4$ configurations, employing $m, n = 1, 2, 3$. Fundamental frequency is carried out with respect to the aspect ratio $a/b$, for magnitude of non local ratio $(\ell/a)^2$ equal to 0.00, 0.05 and 0.10. Materials selected are given by $E_1/E_2$ equal to 25 and 40, $\nu_{12} = 0.25$, $G_{12} = G_{13} = 0.5E_2$.

In Fig. 10, for the classical theory case, it is possible to see a reducing magnitude of dimensionless fundamental frequency which stabilizes for values of $a/b$ between 1 and 2, for every geometrical configuration and material property. This is similar in the initial stage for second-order strain gradient

| $E_1/E_2$ | | | 10 | | | 20 | | |
|---|---|---|---|---|---|---|---|---|
| | m | n | (0/90) | $(0/90)_2$ | $(0/90)_4$ | (0/90) | $(0/90)_2$ | $(0/90)_4$ |
| Reddy [52] | 1 | 1 | 1.183 | 1.479 | 1.545 | 0.990 | 1.386 | 1.469 |
| | 1 | 2 | 3.174 | 4.077 | 4.274 | 2.719 | 3.913 | 4.158 |
| | 1 | 3 | 6.666 | 8.698 | 9.136 | 5.789 | 8.456 | 8.998 |
| | 2 | 1 | 3.174 | 4.077 | 4.274 | 2.719 | 3.913 | 4.158 |
| | 2 | 2 | 4.733 | 5.918 | 6.179 | 3.959 | 5.547 | 5.877 |
| | 2 | 3 | 7.927 | 10.034 | 10.494 | 6.702 | 9.507 | 10.088 |
| | 3 | 1 | 6.666 | 8.698 | 9.136 | 5.789 | 8.456 | 8.998 |
| | 3 | 2 | 7.927 | 10.034 | 10.494 | 6.193 | 9.507 | 10.088 |
| | 3 | 3 | 10.650 | 13.317 | 13.904 | 8.908 | 12.481 | 13.224 |
| $(\ell/a)^2 = 0.00$ | 1 | 1 | 1.183 | 1.480 | 1.545 | 0.990 | 1.387 | 1.469 |
| | 1 | 2 | 3.174 | 4.078 | 4.274 | 2.719 | 3.913 | 4.158 |
| | 1 | 3 | 6.666 | 8.698 | 9.136 | 5.789 | 8.455 | 8.998 |
| | 2 | 1 | 3.174 | 4.078 | 4.274 | 2.719 | 3.913 | 4.158 |
| | 2 | 2 | 4.733 | 5.918 | 6.179 | 3.959 | 5.547 | 5.877 |
| | 2 | 3 | 7.927 | 10.033 | 10.494 | 6.702 | 9.507 | 10.088 |
| | 3 | 1 | 6.666 | 8.698 | 9.136 | 5.789 | 8.455 | 8.998 |
| | 3 | 2 | 7.927 | 10.033 | 10.494 | 6.702 | 9.507 | 10.088 |
| | 3 | 3 | 10.650 | 13.317 | 13.903 | 8.908 | 12.481 | 13.224 |
| $(\ell/a)^2 = 0.05$ | 1 | 1 | 1.888 | 2.132 | 2.189 | 1.625 | 1.999 | 2.082 |
| | 1 | 2 | 7.135 | 7.851 | 8.020 | 6.267 | 7.517 | 7.798 |
| | 1 | 3 | 19.151 | 21.790 | 22.401 | 16.758 | 21.088 | 22.038 |
| | 2 | 1 | 6.159 | 7.642 | 7.969 | 5.338 | 7.335 | 7.754 |
| | 2 | 2 | 12.522 | 13.594 | 13.849 | 11.354 | 12.848 | 13.195 |
| | 2 | 3 | 27.962 | 28.731 | 28.920 | 26.420 | 27.595 | 27.882 |
| | 3 | 1 | 16.487 | 21.238 | 22.268 | 14.343 | 20.638 | 21.931 |
| | 3 | 2 | 23.449 | 27.703 | 28.668 | 20.521 | 26.311 | 27.569 |
| | 3 | 3 | 39.910 | 43.249 | 44.044 | 36.312 | 40.902 | 41.971 |
| $(\ell/a)^2 = 0.10$ | 1 | 1 | 2.333 | 2.614 | 2.679 | 2.023 | 2.452 | 2.548 |
| | 1 | 2 | 9.435 | 10.295 | 10.498 | 8.335 | 9.862 | 10.208 |
| | 1 | 3 | 26.104 | 29.530 | 30.326 | 22.893 | 28.582 | 29.835 |
| | 2 | 1 | 8.058 | 9.998 | 10.426 | 6.985 | 9.597 | 10.145 |
| | 2 | 2 | 16.795 | 18.229 | 18.570 | 15.235 | 17.230 | 17.694 |
| | 2 | 3 | 38.201 | 39.241 | 39.497 | 36.113 | 37.695 | 38.080 |
| | 3 | 1 | 22.313 | 28.742 | 30.136 | 19.411 | 27.930 | 29.680 |
| | 3 | 2 | 32.025 | 37.834 | 39.152 | 28.026 | 35.933 | 37.652 |
| | 3 | 3 | 54.997 | 59.596 | 60.691 | 50.041 | 56.362 | 57.835 |

Table 5: Dimensionless frequncies $\bar{\omega}$ of antisymmetric cross-ply laminates

| $E_1/E_2$ | 25 | | 40 | |
|---|---|---|---|---|
| | $(-45/45)$ | $(-45/45)_4$ | $(45/-45)$ | $(45/-45)_3$ |
| Reddy [52] | 12,357 | 20,154 | 14,636 | 24,825 |
| $(\ell/a)^2 = 0.00$ | 12,358 | 20,154 | 14,636 | 24,825 |
| $(\ell/a)^2 = 0.05$ | 17,419 | 28,409 | 20,631 | 34,994 |
| $(\ell/a)^2 = 0.10$ | 21,311 | 34,756 | 25,241 | 42,812 |

Table 6: Dimensionless frequncies $\bar{\omega}$ of antisymmetric angle-ply laminates

theory, even if for the whole study they show greater magnitude, while they display an increasing trend for values around 1.2 onwards. It is also possible to say that, $\bar{\omega}$ has greater magnitude as the number of the layer of the plate increases accounting for the same thickness and for lower $E_1/E_2$ ratios. Finally, as previously demonstratde dimensionless fundamental frequency increases as $(\ell/a)^2$ rises.

### *4.3. Antisymmetric angle-ply*

The last step of the present paper is focused on the analysis of the antisymmetric angle-ply laminates in terms of dimensionless frequency. Firstly, three different layouts of squared plate are considered: $(-45/45)$, $(-45/45)_4$, $(45/-45)$ and $(45/-45)_4$. The material properties for the first two columns are: $E_1/E_2 = 25$, $\nu_{12} = 0.25$, $G_{12} = G_{13} = 0.5E_2$ and for the last two $E_1/E_2 = 40$, $\nu_{12} = 0.25$, $G_{12} = G_{13} = 0.6E_2$. The frequency is dimensionless as following: $\bar{\omega} = \omega a^2/h\sqrt{\rho/E_2}$ and $n = m = 1$ is considered.

In the first two rows of Tab. 6, the comparison with Reddy [52] for the classical theory was made showing perfect agreement. The third and fourth rows display the extension to the second-order strain gradient theory, for which outcomes have a rising trend with $(\ell/a)^2$ for each case.

Finally, trends by changing $a/b$ (increased from three to five) are drawn in Fig. 11, for $m, n = 1, 2, 3$, in terms of dimensionless fundamental frequency: $\bar{\omega} = \omega b^2/\pi^2\sqrt{\rho h/D_{22}}$. Material properties chosen as $E_1/E_2$ equal to 25 and 40, $\nu_{12} = 0.25$, $G_{12} = G_{13} = 0.5E_2$. The plates configurations that are studied are: $(-45/45)$, $(-45/45)_2$ and $(-45/45)_3$.

In the graph 11 trends similar to the cross-ply case are shown, on the other hand much higher magnitudes of dimensionless fundamental frequencies are reached in the present case. Decreasing in the early phase and then constant behavior is shown for the classical theory ($(\ell/a)^2 = 0.00$), on the contrary a growing behavior by changing $a/b$ if non local effects are taken into account is observed for $(\ell/a)^2 = 0.05$ and $(\ell/a)^2 = 0.10$. It is also displayed as the magnitude of $\bar{\omega}$ grows for a major number of layers in the plate configuration to parity of thickness. The last observation regards the materials, in fact it is clear as $\bar{\omega}$ illustrates a slight more significant impact if the ratio $E_1/E_2$ is equal to 25.

## 5. Conclusion

In the present paper, the stability and dynamic analysis of simply supported nano plates are examined, applying the Kirchhoff theory and Navier solution method. An assortment of plate layouts, materials and geometries are involved, comparisons for the classical case wherever it was possible are provided, then outcomes are extended to the second-order strain gradient theory, thus taking into account nonlocal effects.

Firstly, making an analogy between laminates, for both cross- and angle-ply, in uniaxial and biaxial cases, it is clear that it is possible to exploit the higher resistance of orthotropic angle-ply plates against buckling issues compared to the cross-ply plates. Moreover, for what concerns the dimensions of the laminate in order to avoid early collapse it is needed to avoid $a/b$ close to one, when higher order theory is employed to catch the nano plates behavior. Also, in the same material and geometrical conditions, it is preferable to use plates made by more layers to parity of plate thickness.

Finally, the procedure applied for the dynamic analysis shows non linear trends for cross- and angle-ply laminates by changing plate aspect ratios. Moreover, in this case it is also shown the much higher magnitude in terms of dimensionless fundamental frequency if angle-ply plates are employed. Also, for a defined plate thickness, the application of a greater number of layers, as well as the use of material with lower ratio $E_1/E_2$ induces to more considerable values of dimensioless frequencey of the structure.

In conclusion, from this study comes out that the performance of the second-order strain gradient theory is differerent from the classical one on by far, and the gap increases with plate aspect ratio and with non local ratio, thus nano plates need to be analyzed by considering non local effects.

## Appendix A. Appendix

Differential operators of the Hamilton's Principle are explicitly given below, where $f$ indicates the generic derivative operator to be applied for the partial derivation (for instance $f_{,x} = \frac{\partial}{\partial x}$):

$$\mathcal{T}_{11} = A_{11} f_{,x} + A_{16} f_{,y} - \ell^2 \left[ A_{11}\left( f_{,xxx} + f_{,xyy} \right) + A_{16}\left( f_{,xyy} + f_{,yyy} \right) \right] \quad \text{(A.1)}$$

$$\mathcal{T}_{12} = A_{12}f_{,y} + A_{16}f_{,x} - \ell^2\left[A_{12}\left(f_{,yyy} + f_{,xxy}\right) + A_{16}\left(f_{,xyy} + f_{,xxx}\right)\right] \quad (A.2)$$

$$\begin{aligned}\mathcal{T}_{13} = &-\left(B_{11}f_{,xx} + B_{12}f_{,yy} + 2B_{16}f_{,xy}\right) + \ell^2\Big[B_{11}\left(f_{,xxxx} + f_{,xxyy}\right) + \\ &+ B_{12}\left(f_{,xxyy} + f_{,yyyy}\right) + 2B_{16}\left(f_{,xxxy} + f_{,xyyy}\right)\Big]\end{aligned} \quad (A.3)$$

$$\mathcal{T}_{21} = A_{16}f_{,x} + A_{66}f_{,y} - \ell^2\left[A_{16}\left(f_{,xxx} + f_{,xyy}\right) + A_{66}\left(f_{,xxy} + f_{,yyy}\right)\right] = \mathcal{T}_{31} \quad (A.4)$$

$$\mathcal{T}_{22} = A_{26}f_{,y} + A_{66}f_{,x} - \ell^2\left[A_{26}\left(f_{,yyy} + f_{,xxy}\right) + A_{66}\left(f_{,xyy} + f_{,xxx}\right)\right] = \mathcal{T}_{32} \quad (A.5)$$

$$\begin{aligned}\mathcal{T}_{23} = &-\left(B_{16}f_{,xx} + B_{26}f_{,yy} + 2B_{66}f_{,xy}\right) + \ell^2\Big[B_{16}\left(f_{,xxxx} + f_{,xxyy}\right) + \\ &+ B_{26}\left(f_{,xxyy} + f_{,yyyy}\right) + 2B_{66}\left(f_{,xxxy} + f_{,xyyy}\right)\Big] = \mathcal{T}_{33}\end{aligned} \quad (A.6)$$

$$\mathcal{T}_{31} = A_{16}f_{,x} + A_{66}f_{,y} - \ell^2\left[A_{16}\left(f_{,xxx} + f_{,xyy}\right) + A_{66}\left(f_{,xxy} + f_{,yyy}\right)\right] \quad (A.7)$$

$$\mathcal{T}_{32} = A_{26}f_{,y} + A_{66}f_{,x} - \ell^2\left[A_{26}\left(f_{,yyy} + f_{,xxy}\right) + A_{66}\left(f_{,xyy} + f_{,xxx}\right)\right] \quad (A.8)$$

$$\mathcal{T}_{33} = -\left(B_{16}f_{,xx} + B_{26}f_{,yy} + 2B_{66}f_{,xy}\right) + \ell^2\Bigg[B_{16}\left(f_{,xxxx} + f_{,xxyy}\right) + \\ + B_{26}\left(f_{,xxyy} + f_{,yyyy}\right) + 2B_{66}\left(f_{,xxxy} + f_{,xyyy}\right)\Bigg] \tag{A.9}$$

$$\mathcal{T}_{41} = A_{12}f_{,x} + A_{26}f_{,y} - \ell^2\left[A_{12}\left(f_{,xxx} + f_{,xyy}\right) + A_{26}\left(f_{,xxy} + f_{,yyy}\right)\right] \tag{A.10}$$

$$\mathcal{T}_{42} = A_{22}f_{,y} + A_{26}f_{,x} - \ell^2\left[A_{22}\left(f_{,yyy} + f_{,xxy}\right) + A_{26}\left(f_{,xxy} + f_{,yyy}\right)\right] \tag{A.11}$$

$$\mathcal{T}_{43} = -\left(B_{12}f_{,xx} + B_{22}f_{,yy} + 2B_{26}f_{,xy}\right) + \ell^2\Bigg[B_{12}\left(f_{,xxxx} + f_{,xxyy}\right) + \\ + B_{22}\left(f_{,xxyy} + f_{,yyyy}\right) + 2B_{26}\left(f_{,xyyy} + f_{,xxxy}\right)\Bigg] \tag{A.12}$$

$$\mathcal{T}_{51} = -\left(B_{11}f_{,x} + B_{16}f_{,y}\right) + \ell^2\left[B_{11}\left(f_{,xxx} + f_{,xyy}\right) + B_{16}\left(f_{,xxy} + f_{,yyy}\right)\right] \tag{A.13}$$

$$\mathcal{T}_{52} = -\left(B_{12}f_{,y} + B_{16}f_{,x}\right) + \ell^2\left[B_{12}\left(f_{,yyy} + f_{,xxy}\right) + B_{16}\left(f_{,xyy} + f_{,xxx}\right)\right] \tag{A.14}$$

$$\mathcal{T}_{53} = D_{11}f_{,xx} + D_{12}f_{,yy} + 2D_{16}f_{,xy} - \ell^2\Bigg[D_{11}\left(f_{,xxxx} + f_{,xxyy}\right) + \\ + D_{12}\left(f_{,xxyy} + f_{,yyyy}\right) + 2D_{16}\left(f_{,xyyy} + f_{,xxxy}\right)\Bigg] \tag{A.15}$$

$$\mathcal{T}_{61} = -\Big(B_{12}f_{,x} + B_{26}f_{,y}\Big) + \ell^2\Big[B_{12}\Big(f_{,xxx} + f_{,xyy}\Big) + B_{26}\Big(f_{,xxy} + f_{,yyy}\Big)\Big] \tag{A.16}$$

$$\mathcal{T}_{62} = -\Big(B_{22}f_{,y} + B_{26}f_{,x}\Big) + \ell^2\Big[B_{22}\Big(f_{,yyy} + f_{,xxy}\Big) + B_{26}\Big(f_{,xyy} + f_{,xxx}\Big)\Big] \tag{A.17}$$

$$\begin{aligned}\mathcal{T}_{63} = D_{12}f_{,xx} + D_{22}f_{,yy} + 2D_{26}f_{,xy} - \ell^2\Big[D_{12}\Big(f_{,xxxx} + f_{,xxyy}\Big)\\ + D_{22}\Big(f_{,xxyy} + f_{,yyyy}\Big) + 2D_{26}\Big(f_{,xyyy} + f_{,xxxy}\Big)\Big]\end{aligned} \tag{A.18}$$

$$\begin{aligned}\mathcal{T}_{71} = 2\Big[-\Big(B_{16}f_{,x} + B_{66}f_{,y}\Big) + \ell^2\Big(B_{16}\Big(f_{,xxx} + f_{,xyy}\Big)\\ + B_{66}\Big(f_{,xxy} + f_{,yyy}\Big)\Big)\Big]\end{aligned} \tag{A.19}$$

$$\begin{aligned}\mathcal{T}_{72} = 2\Big[-\Big(B_{26}f_{,y} + B_{66}f_{,x}\Big) + \ell^2\Big(B_{26}\Big(f_{,yyy} + f_{,xxy}\Big)\\ + B_{66}\Big(f_{,xyy} + f_{,xxx}\Big)\Big)\Big]\end{aligned} \tag{A.20}$$

$$\begin{aligned}\mathcal{T}_{73} = 2\Big[D_{16}f_{,xx} + D_{26}f_{,yy} + 2D_{66}f_{,xy} - \ell^2\Big(D_{16}\Big(f_{,xxxx} + f_{,xxyy}\Big)\\ + D_{26}\Big(f_{,xxyy} + f_{,yyyy}\Big) + 2D_{66}\Big(f_{,xyyy} + f_{,xxxy}\Big)\Big]\end{aligned} \tag{A.21}$$

## References


[1] C. Li, E. T. Thostenson, T.-W. Chou, Sensors and actuators based on carbon nanotubes and their composites: a review, Composites science and technology 68 (2008) 1227–1249.

[2] K. Ekinci, M. Roukes, Nanoelectromechanical systems, Review of scientific instruments 76 (2005) 061101.

[3] M. Mohammadimehr, H. M. Hooyeh, H. Afshari, M. R. Salarkia, Free vibration analysis of double-bonded isotropic piezoelectric timoshenko microbeam based on strain gradient and surface stress elasticity theories under initial stress using differential quadrature method, Mechanics of Advanced Materials and Structures 24 (2017) 287–303.

[4] R. Barretta, L. Feo, R. Luciano, F. M. de Sciarra, A gradient eringen model for functionally graded nanorods, Composite Structures 131 (2015) 1124–1131.

[5] B. Bhushan, Nanotribology and nanomechanics of mems/nems and biomems/bionems materials and devices, Microelectronic Engineering 84 (2007) 387–412.

[6] D. Berman, J. Krim, Surface science, mems and nems: Progress and opportunities for surface science research performed on, or by, microdevices, Progress in Surface Science 88 (2013) 171–211.

[7] V. S. Saji, H. C. Choe, K. W. Yeung, Nanotechnology in biomedical applications: a review, International Journal of Nano and Biomaterials 3 (2010) 119–139.

[8] P. Sharma, S. Ganti, N. Bhate, Effect of surfaces on the size-dependent elastic state of nano-inhomogeneities, Applied Physics Letters 82 (2003) 535–537.

[9] B. Wang, S. Zhou, J. Zhao, X. Chen, A size-dependent kirchhoff micro-plate model based on strain gradient elasticity theory, European Journal of Mechanics - A/Solids 30 (2011) 517 – 524.

[10] A. Li, S. Zhou, S. Zhou, B. Wang, A size-dependent model for bi-layered kirchhoff micro-plate based on strain gradient elasticity theory, Composite Structures 113 (2014) 272 – 280.

[11] B. Akgöz, Ö. Civalek, A microstructure-dependent sinusoidal plate model based on the strain gradient elasticity theory, Acta Mechanica 226 (2015) 2277–2294.

[12] M. R. Barati, N. M. Faleh, A. M. Zenkour, Dynamic response of nanobeams subjected to moving nanoparticles and hygro-thermal environments based on nonlocal strain gradient theory, Mechanics of Advanced Materials and Structures 0 (2018) 1–9.

[13] A. W. McFarland, J. S. Colton, Role of material microstructure in plate stiffness with relevance to microcantilever sensors, Journal of Micromechanics and Microengineering 15 (2005) 1060.

[14] D. C. Lam, F. Yang, A. Chong, J. Wang, P. Tong, Experiments and theory in strain gradient elasticity, Journal of the Mechanics and Physics of Solids 51 (2003) 1477–1508.

[15] J. S. Stölken, A. Evans, A microbend test method for measuring the plasticity length scale, Acta Materialia 46 (1998) 5109–5115.

[16] J. H. Lii, N. L. Allinger, Molecular mechanics. the mm3 force field for hydrocarbons. 3. the van der waals' potentials and crystal data for aliphatic and aromatic hydrocarbons, Journal of the American Chemical Society 111 (1989) 8576–8582.

[17] N. L. Allinger, Conformational analysis. 130. mm2. a hydrocarbon force field utilizing v1 and v2 torsional terms, Journal of the American Chemical Society 99 (1977) 8127–8134.

[18] J. Tersoff, New empirical approach for the structure and energy of covalent systems, Physical Review B 37 (1988) 6991.

[19] D. W. Brenner, Empirical potential for hydrocarbons for use in simulating the chemical vapor deposition of diamond films, Physical review B 42 (1990) 9458.

[20] A. Ashoori, M. J. Mahmoodi, A nonlinear thick plate formulation based on the modified strain gradient theory, Mechanics of Advanced Materials and Structures 25 (2018) 813–819.

[21] B. Babu, B. Patel, A new computationally efficient finite element formulation for nanoplates using second-order strain gradient kirchhoff's plate theory, Composites Part B: Engineering 168 (2019) 302–311.

[22] M. Hosseini, A. Jamalpoor, A. Fath, Surface effect on the biaxial buckling and free vibration of fgm nanoplate embedded in visco-pasternak

standard linear solid-type of foundation, Meccanica 52 (2017) 1381–1396.

[23] B. Akgöz, Ö. Civalek, Bending analysis of embedded carbon nanotubes resting on an elastic foundation using strain gradient theory, Acta Astronautica 119 (2016) 1–12.

[24] Ç. Demir, Ö. Civalek, On the analysis of microbeams, International Journal of Engineering Science 121 (2017) 14–33.

[25] B. Akgöz, Ö. Civalek, Bending analysis of fg microbeams resting on winkler elastic foundation via strain gradient elasticity, Composite Structures 134 (2015) 294–301.

[26] A. C. Eringen, Nonlocal polar elastic continua, International journal of engineering science 10 (1972) 1–16.

[27] K. Lazopoulos, On bending of strain gradient elastic micro-plates, Mechanics Research Communications 36 (2009) 777 – 783.

[28] A. A. Movassagh, M. Mahmoodi, A micro-scale modeling of kirchhoff plate based on modified strain-gradient elasticity theory, European Journal of Mechanics - A/Solids 40 (2013) 50 – 59.

[29] M. Mirsalehi, M. Azhari, H. Amoushahi, Buckling and free vibration of the fgm thin micro-plate based on the modified strain gradient theory and the spline finite strip method, European Journal of Mechanics - A/Solids 61 (2017) 1 – 13.

[30] C. Li, L. Yao, W. Chen, S. Li, Comments on nonlocal effects in nano-cantilever beams, International Journal of Engineering Science 87 (2015) 47–57.

[31] B. Akgöz, Ö. Civalek, Analysis of micro-sized beams for various boundary conditions based on the strain gradient elasticity theory, Archive of Applied Mechanics 82 (2012) 423–443.

[32] A. C. Eringen, On differential equations of nonlocal elasticity and solutions of screw dislocation and surface waves, Journal of applied physics 54 (1983) 4703–4710.

[33] E. C. Aifantis, On the role of gradients in the localization of deformation and fracture, International Journal of Engineering Science 30 (1992) 1279–1299.

[34] S. Altan, E. Aifantis, On the structure of the mode iii crack-tip in gradient elasticity, Scripta Metallurgica et Materialia 26 (1992) 319–324.

[35] C. Ru, E. Aifantis, A simple approach to solve boundary-value problems in gradient elasticity, Acta Mechanica 101 (1993) 59–68.

[36] C. S. Chang, J. Gao, Second-gradient constitutive theory for granular material with random packing structure, International Journal of Solids and Structures 32 (1995) 2279–2293.

[37] H. Mühlhaus, F. Oka, Dispersion and wave propagation in discrete and continuous models for granular materials, International Journal of Solids and Structures 33 (1996) 2841–2858.

[38] F. Yang, A. Chong, D. C. C. Lam, P. Tong, Couple stress based strain gradient theory for elasticity, International Journal of Solids and Structures 39 (2002) 2731–2743.

[39] F. Ebrahimi, M. R. Barati, Vibration analysis of biaxially compressed double-layered graphene sheets based on nonlocal strain gradient theory, Mechanics of Advanced Materials and Structures 26 (2019) 854–865.

[40] Y. Li, Z. Cai, S. Shi, Buckling and free vibration of magnetoelectroelastic nanoplate based on nonlocal theory, Composite Structures 111 (2014) 522 – 529.

[41] A. Farajpour, M. Danesh, M. Mohammadi, Buckling analysis of variable thickness nanoplates using nonlocal continuum mechanics, Physica E: Low-dimensional Systems and Nanostructures 44 (2011) 719 – 727.

[42] T. Aksencer, M. Aydogdu, Levy type solution method for vibration and buckling of nanoplates using nonlocal elasticity theory, Physica E: Low-dimensional Systems and Nanostructures 43 (2011) 954 – 959.

[43] Z. Yan, L. Y. Jiang, Vibration and buckling analysis of a piezoelectric nanoplate considering surface effects and in-plane constraints, Proceedings of the Royal Society A: Mathematical, Physical and Engineering Sciences 468 (2012) 3458–3475.

[44] H. B. Khaniki, S. Hosseini-Hashemi, Dynamic response of biaxially loaded double-layer viscoelastic orthotropic nanoplate system under a moving nanoparticle, International Journal of Engineering Science 115 (2017) 51 – 72.

[45] K. Kiani, Small-scale effect on the vibration of thin nanoplates subjected to a moving nanoparticle via nonlocal continuum theory, Journal of Sound and Vibration 330 (2011) 4896 – 4914.

[46] R. Kolahchi, H. Hosseini, M. Esmailpour, Differential cubature and quadrature-bolotin methods for dynamic stability of embedded piezoelectric nanoplates based on visco-nonlocal-piezoelasticity theories, Composite Structures 157 (2016) 174 – 186.

[47] A. Assadi, B. Farshi, A. Alinia-Ziazi, Size dependent dynamic analysis of nanoplates, Journal of Applied Physics 107 (2010) 124310.

[48] S. Rajasekaran, H. B. Khaniki, Finite element static and dynamic analysis of axially functionally graded nonuniform small-scale beams based on nonlocal strain gradient theory, Mechanics of Advanced Materials and Structures 26 (2019) 1245–1259.

[49] R. Kolahchi, M. S. Zarei, M. H. Hajmohammad, A. N. Oskouei, Visco-nonlocal-refined zigzag theories for dynamic buckling of laminated nanoplates using differential cubature-bolotin methods, Thin-Walled Structures 113 (2017) 162 – 169.

[50] S. Papargyri-Beskou, D. E. Beskos, Static, stability and dynamic analysis of gradient elastic flexural kirchhoff plates, Archive of Applied Mechanics 78 (2008) 625–635.

[51] F. Cornacchia, N. Fantuzzi, R. Luciano, R. Penna, Solution for cross- and angle-ply laminated kirchhoff nano plates in bending using strain gradient theory, Composites Part B: Engineering (2019) 107006.

[52] J. Reddy, Mechanics of Laminated Composite Plates and Shells: Theory and Analysis, Second Edition, CRC Press, 2004.

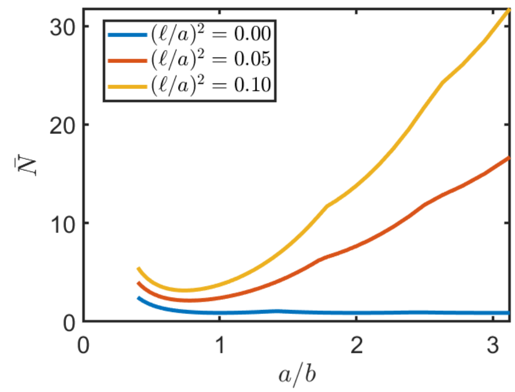


a) (0/90), $E_1/E_2 = 25$

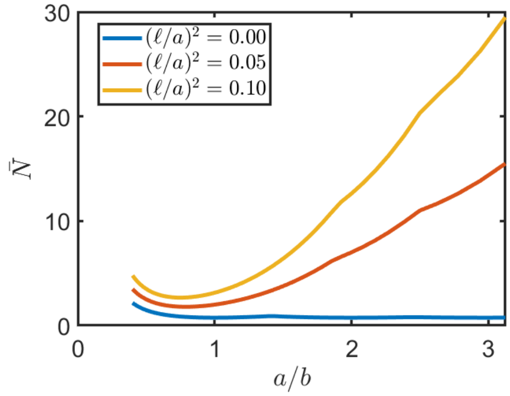


b) (0/90), $E_1/E_2 = 40$

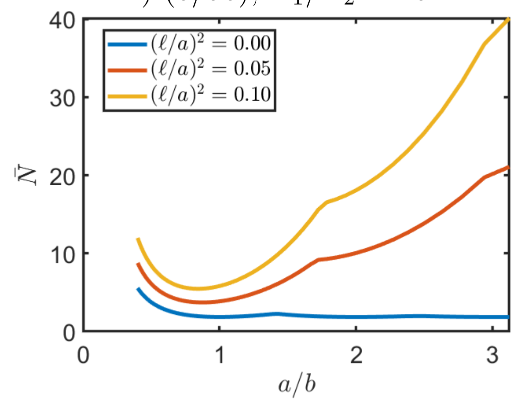


c) $(0/90)_2$, $E_1/E_2 = 25$

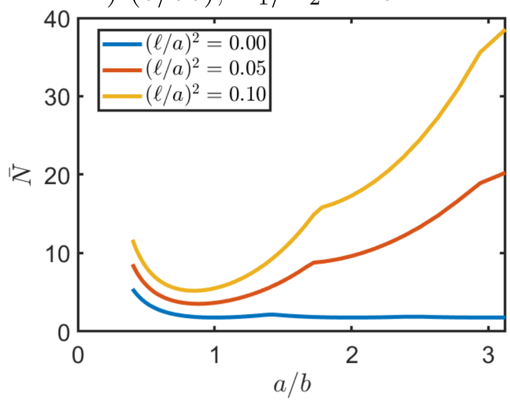


d) $(0/90)_2$, $E_1/E_2 = 40$

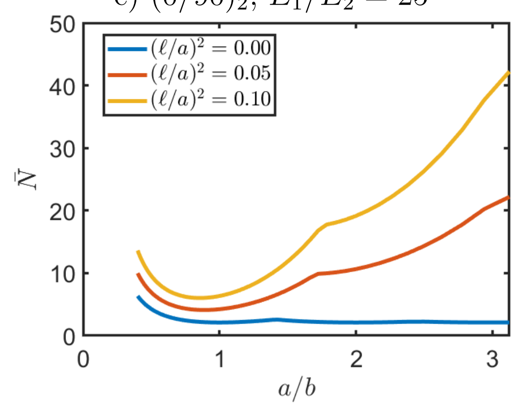


e) $(0/90)_4$, $E_1/E_2 = 25$

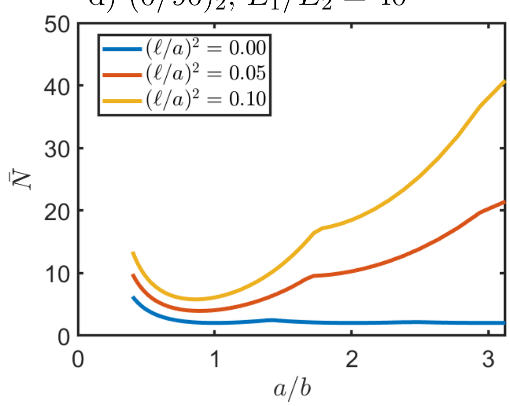


f) $(0/90)_4$, $E_1/E_2 = 40$

Figure 4: Uniaxial buckling load versus aspect ratio

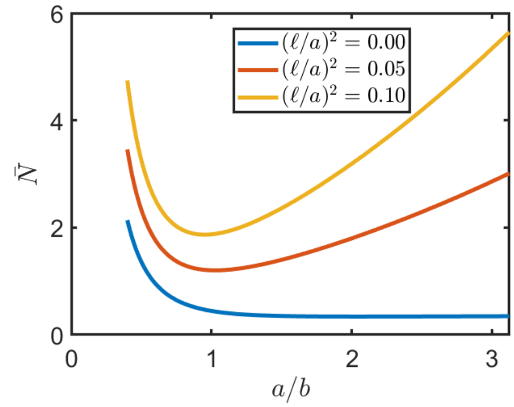


a) (0/90), $E_1/E_2 = 25$

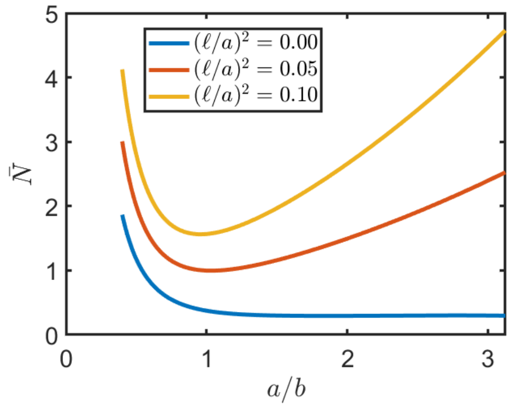


b) (0/90), $E_1/E_2 = 40$

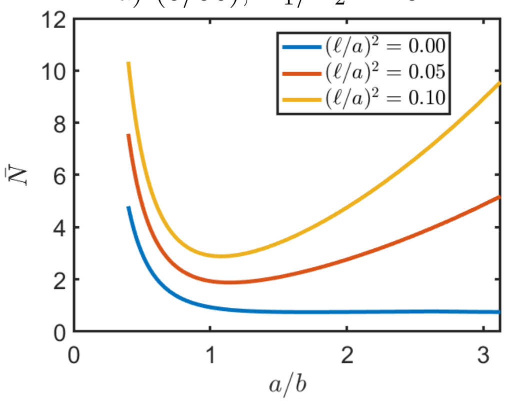


c) $(0/90)_2$, $E_1/E_2 = 25$

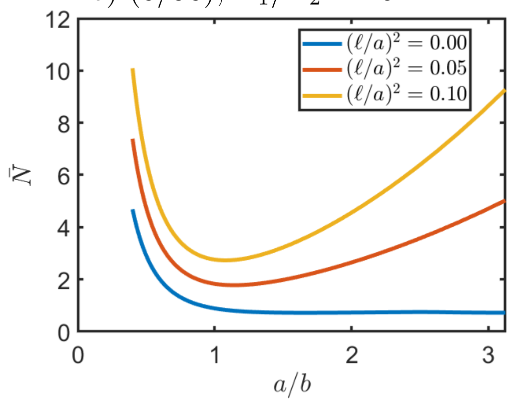


d) $(0/90)_2$, $E_1/E_2 = 40$

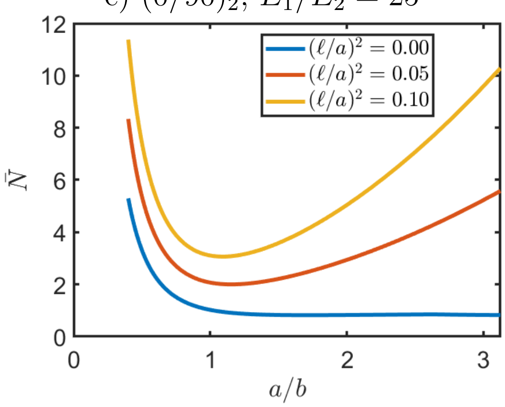


e) $(0/90)_3$, $E_1/E_2 = 25$

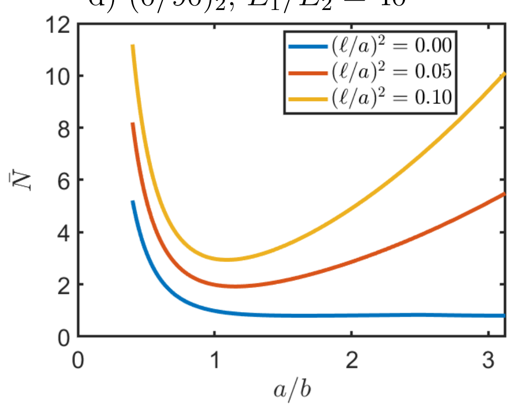


f) $(0/90)_3$, $E_1/E_2 = 40$

Figure 5: Biaxial buckling load versus aspect ratio

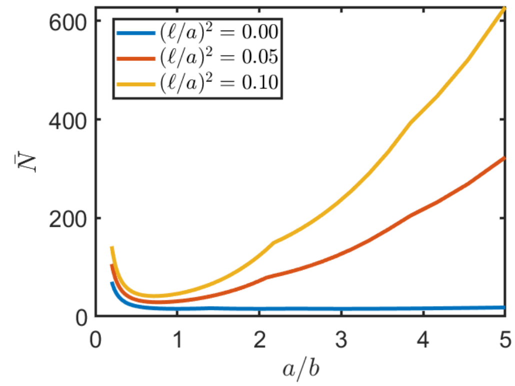


a) $(-45/45)$, $E_1/E_2 = 25$

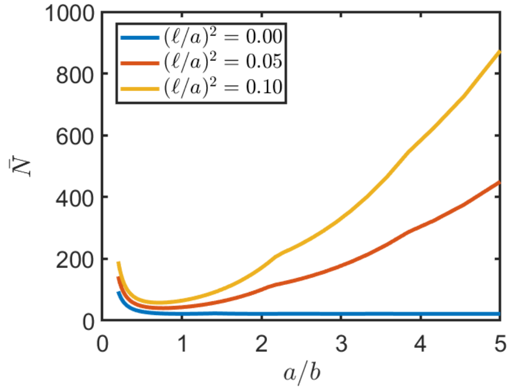


b) $(-45/45)$, $E_1/E_2 = 40$

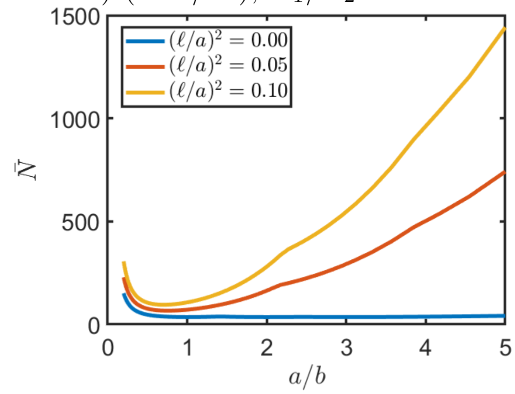


c) $(-45/45)_2$, $E_1/E_2 = 25$

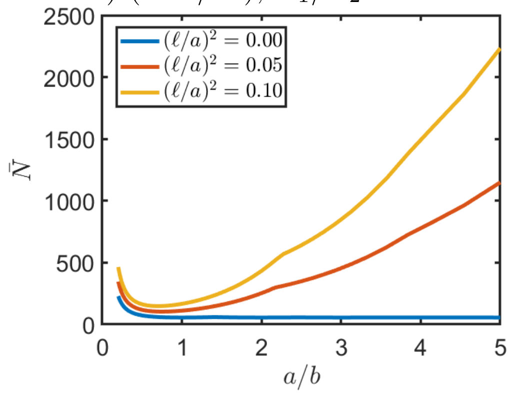


d) $(-45/45)_2$, $E_1/E_2 = 40$

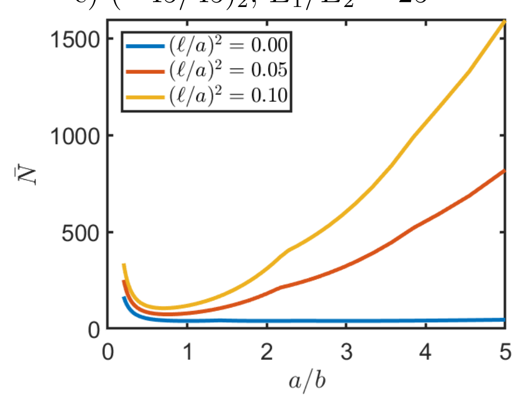


e) $(-45/45)_3$, $E_1/E_2 = 25$

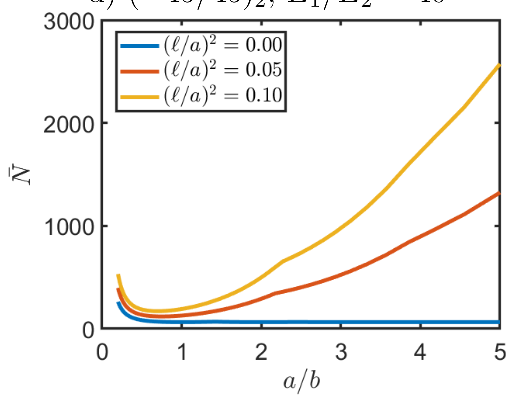


f) $(-45/45)_3$, $E_1/E_2 = 40$

Figure 6: Uniaxial buckling load versus aspect ratio

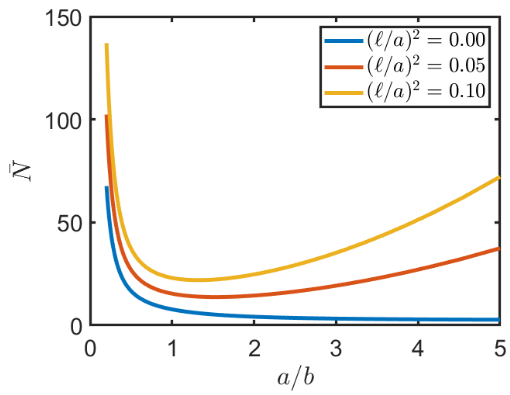


a) $(-45/45)$, $E_1/E_2 = 25$

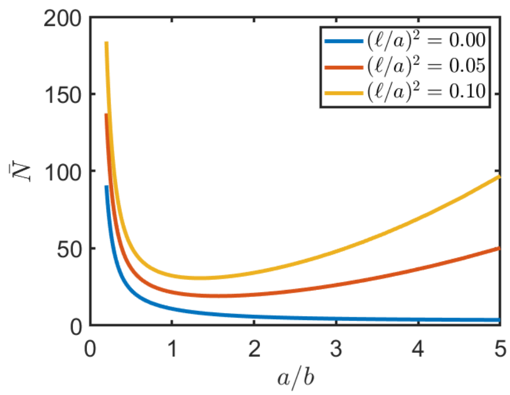


b) $(-45/45)$, $E_1/E_2 = 40$

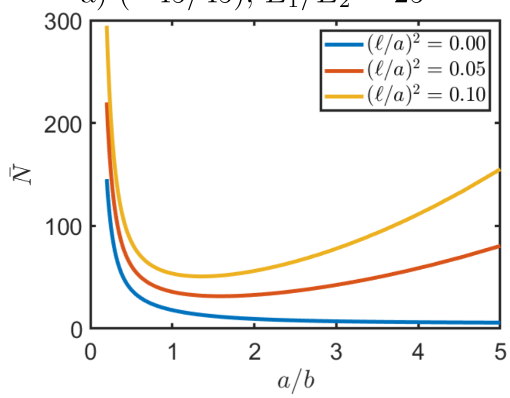


c) $(-45/45)_2$, $E_1/E_2 = 25$

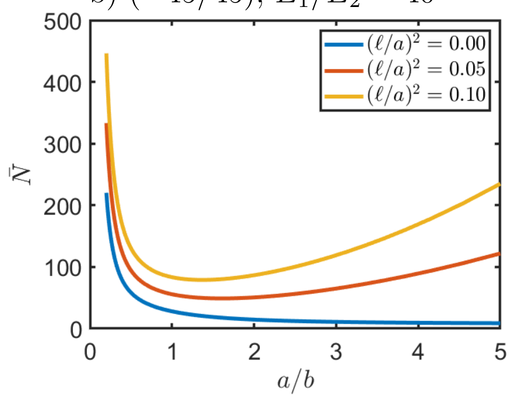


d) $(-45/45)_2$, $E_1/E_2 = 40$

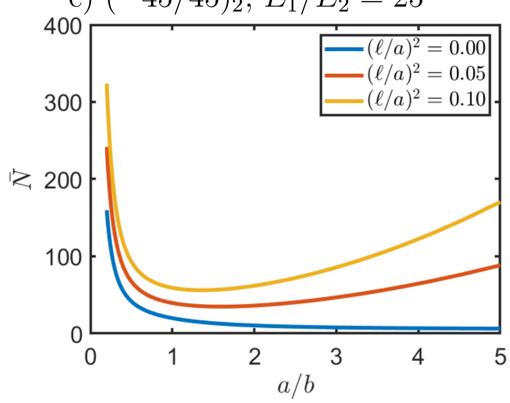


e) $(-45/45)_3$, $E_1/E_2 = 25$

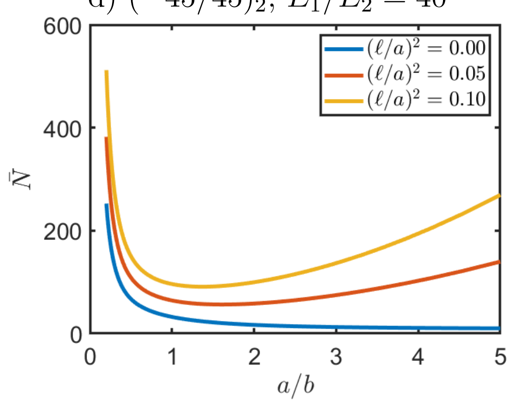


f) $(-45/45)_3$, $E_1/E_2 = 40$

Figure 7: Biaxial buckling load versus aspect ratio

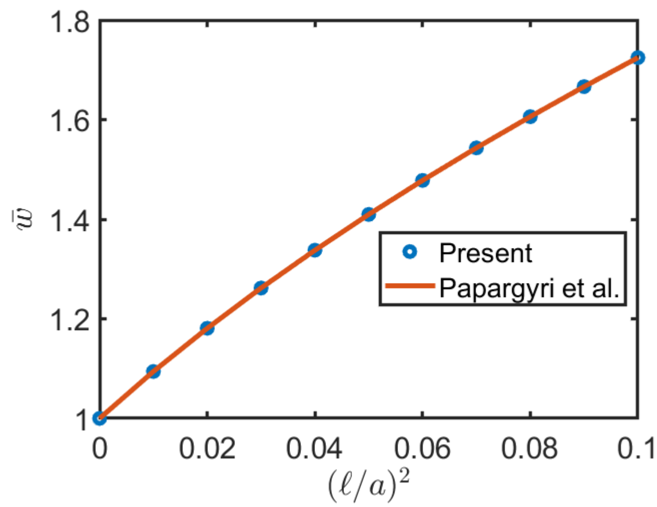


Figure 8: Vibrations - comparison with ref. [50].

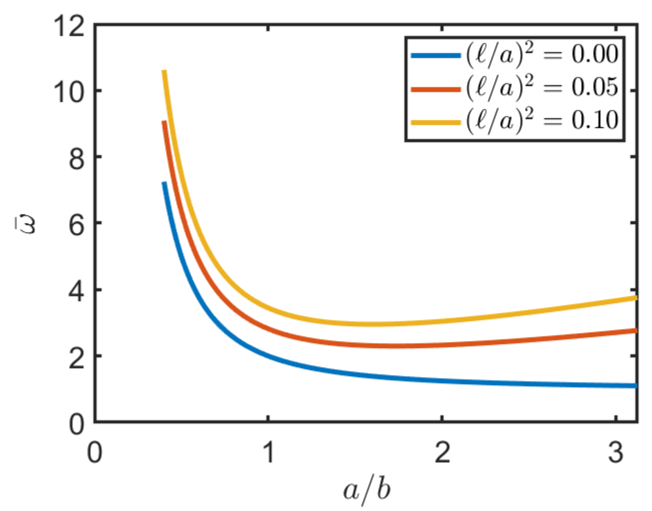


Figure 9: Nondimensionalized fundamental frequency load versus plate aspect ratio for isotropic lamina

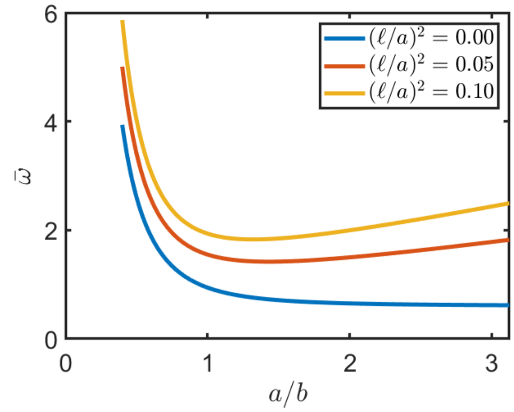


a) (0/90), $E_1/E_2 = 25$

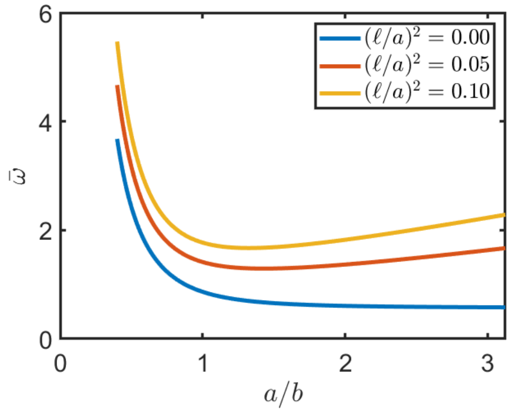


b) (0/90), $E_1/E_2 = 40$

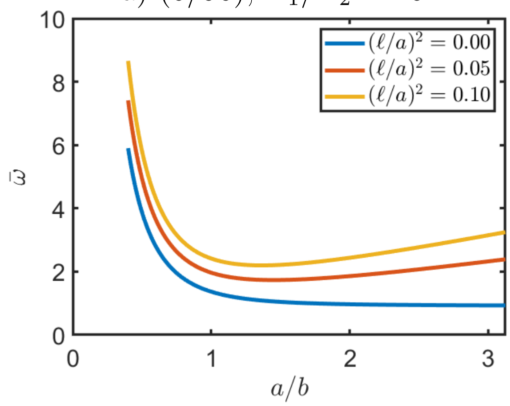


a) $(0/90)_2$, $E_1/E_2 = 25$

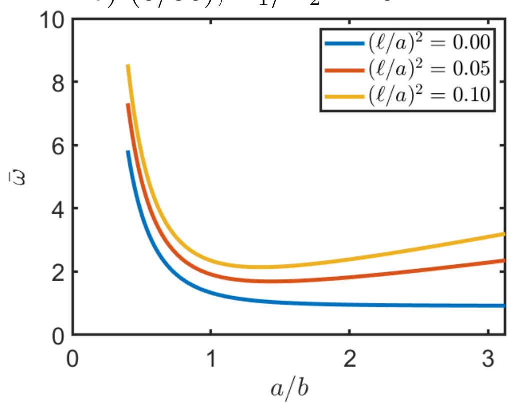


b) $(0/90)_2$, $E_1/E_2 = 40$

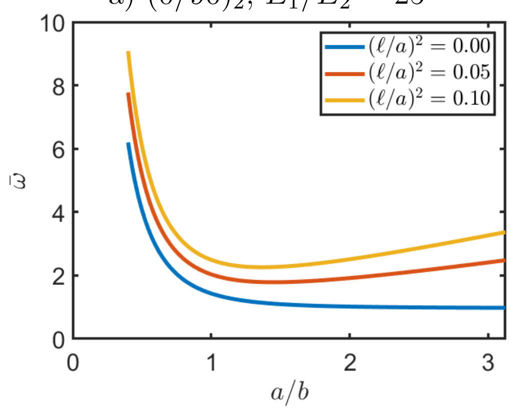


a) $(0/90)_3$, $E_1/E_2 = 25$

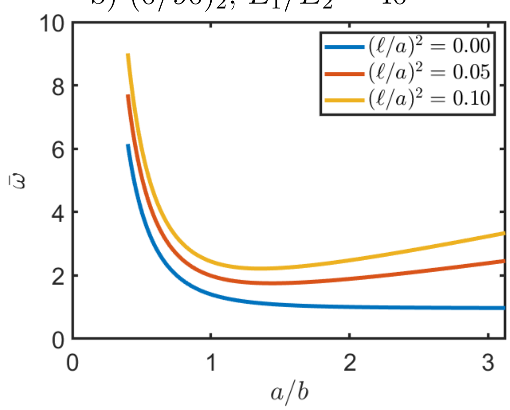


b) $(0/90)_3$, $E_1/E_2 = 40$

Figure 10: Dimensionless fundamental frequency versus plate aspect ratio for antisymmetric cross-ply laminates to changing non local ratios

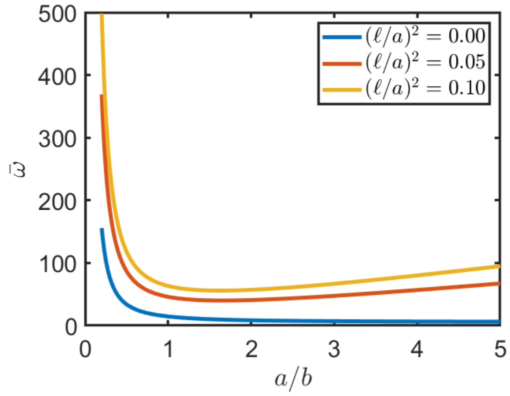


a) $(-45/45)$, $E_1/E_2 = 25$

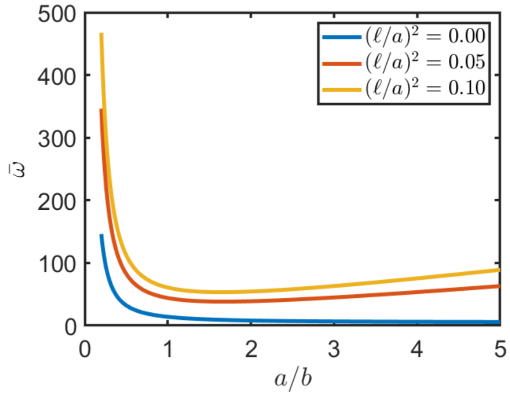


b) $(-45/45)$, $E_1/E_2 = 40$

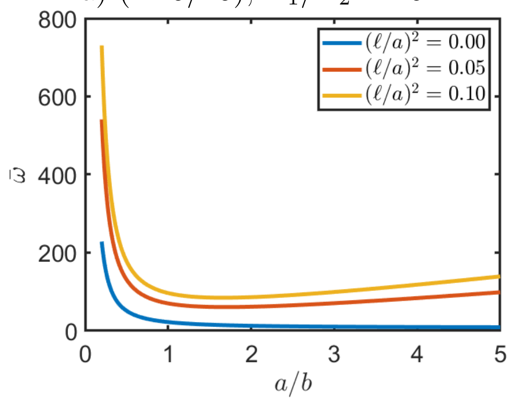


a) $(-45/45)_2$, $E_1/E_2 = 25$

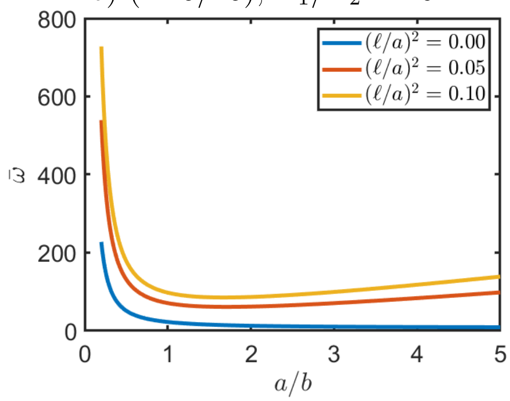


b) $(-45/45)_2$, $E_1/E_2 = 40$

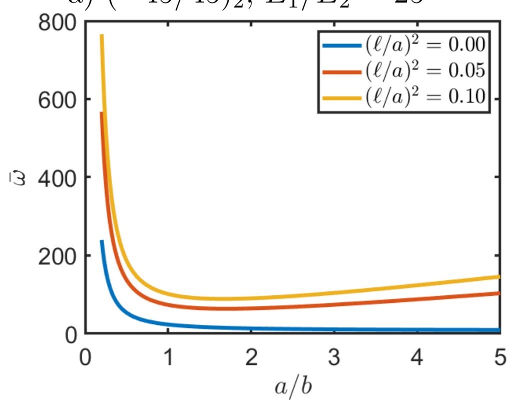


a) $(-45/45)_3$, $E_1/E_2 = 25$

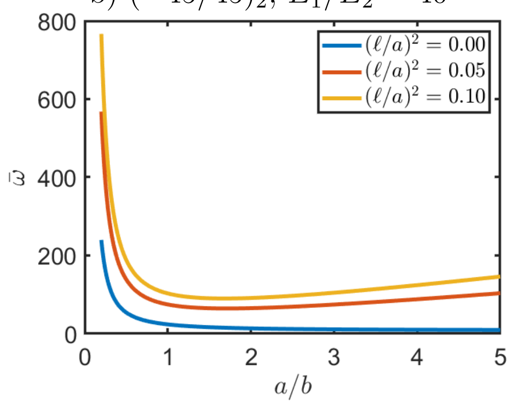


b) $(-45/45)_3$, $E_1/E_2 = 40$

Figure 11: Dimensionless fundamental frequency versus plate aspect ratio for antisymmetric angle-ply laminates to changing non local ratios